Author Manuscript

Author Manuscript

Author Manuscript

Author Manuscript

HHS Public Access

Author manuscript

Biomaterials. Author manuscript; available in PMC 2021 May 10.

Published in final edited form as:

Biomaterials. 2021 January ; 268: 120535. doi:10.1016/j.biomaterials.2020.120535.

Matrix metalloproteinase (MMP)-degradable tissue engineered periosteum coordinates allograft healing via early stage recruitment and support of host neurovasculature

Yiming Li[1,2], **Michael D. Hoffman**[1,2], **Danielle S.W. Benoit**[1,2,3,4,5,6]

[1]Department of Biomedical Engineering, University of Rochester, Rochester, NY, USA

[2]Department of Orthopaedics and Center for Musculoskeletal Research, University of Rochester Medical Center, Rochester, NY, USA

[3]Department of Environmental Medicine, University of Rochester Medical Center, Rochester, NY

[4]Materials Science Program, University of Rochester, Rochester, NY, USA

[5]Department of Chemical Engineering, University of Rochester, Rochester, NY, USA

[6]Department of Biomedical Genetics and Center for Oral Biology, University of Rochester Medical Center, Rochester, NY, USA

Abstract

Despite serving as the clinical “gold standard” treatment for critical size bone defects, decellularized allografts suffer from long-term failure rates of ~60% due to the absence of the periosteum. Stem and osteoprogenitor cells within the periosteum orchestrate autograft healing through host cell recruitment, which initiates the regenerative process. To emulate periosteum-mediated healing, tissue engineering approaches have been utilized with mixed outcomes. While vascularization has been widely established as critical for bone regeneration, innervation was recently identified to be spatiotemporally regulated together with vascularization and similarly indispensable to bone healing. Notwithstanding, there are no known approaches that have focused on periosteal matrix cues to coordinate host vessel and/or axon recruitment. Here, we investigated the influence of hydrogel degradation mechanism, *i.e.* hydrolytic or enzymatic (cell-dictated), on tissue engineered periosteum (TEP)-modified allograft healing, especially host vessel/nerve recruitment and integration. Matrix metalloproteinase (MMP)-degradable hydrogels supported endothelial cell migration from encapsulated spheroids whereas no migration was observed in hydrolytically degradable hydrogels *in vitro,* which correlated with increased neurovascularization *in vivo*. Specifically, ~2.45 and 1.84-fold, and ~3.48 and 2.58-fold greater vessel and nerve densities with high levels of vessel and nerve co-localization was observed using MMP degradable TEP (MMP-TEP) -modified allografts versus unmodified and hydrolytically degradable TEP (Hydro-TEP)-modified allografts, respectively, at 3 weeks post-surgery. MMP-TEP-modified allografts exhibited greater longitudinal graft-localized vascularization and endochondral ossification, along with 4-fold and 2-fold greater maximum torques versus unmodified and Hydro-TEP-modified allografts after 9 weeks, respectively, which was comparable to that of autografts. In summary, our results demonstrated that the MMP-TEP coordinated allograft healing via early stage recruitment and support the recruitment of host neurovasculature. Future directions involve

Author Manuscript Author Manuscript Author Manuscript Author Manuscript

investigating and optimizing the engineered TEP matrix to further emulate periosteal-mediated healing.

1. Introduction

Bone is the second most commonly transplanted tissue after blood.[1] More than one million bone grafts are performed annually in the United States with this number predicted to increase to 1.5 million by 2026.[2] Bone graft transplantation is required to treat critically sized bone defects resulting from trauma, tumors, or abnormal skeletal development.[3] Autografts cannot be used for massive bone defects due to volumetric constraints and associated donor site morbidity[4]. In contrast, processed cadaveric allografts are readily available and fill the need for large volumes of graft material and also obviates donor site pain and morbidity[5]. Allografts can also be shaped in the surgical suite to ensure proper defect placement, are osteoconductive, and offer similar mechanical support to live bone.[6, 7] Additionally, the decellularization of allografts minimizes the possibility of immune rejection and a reduces the risk of disease transmission.[8] Therefore, decellularized bone allografts are considered the clinical "gold standard" of treatment for critically-sized bone defects. However, allografts suffer a 60%, 10-year post-implantation failure rate, which can be attributed to the absence of the periosteum.[6, 9, 10] Bone callus formation at bone autografts devoid of periosteum is ~3.5-fold lower compared to intact autografts and marrow-free autografts at 14 days post-surgery in critically-sized murine femur defects.[11]

The periosteum is composed of an outer fibrous layer, containing fibroblasts, collagen and elastin fibers, and micro vessels and an inner cambium layer containing mesenchymal-like periosteal stem cells, and osteoprogenitors (OPs).[12] After injury, cells within the periosteum rapidly proliferate and secrete cytokines (*e.g.,* IL-1β, IL-6 and TNF-α)[13, 14] and bone morphogenetic proteins (BMPs)[15] to recruit host cells and stimulate angiogenesis and osteogenesis[16, 17]. Later, during callus formation, periosteal and recruited mesenchymal stem cells differentiate into chondrocytes and osteoblasts to form the soft and hard callus, respectively.[18]

Numerous tissue engineering approaches have been taken to imitate periosteum-mediated autograft healing, which can be categorized by cell and/or growth factor delivery.[19–26] However, exogenous growth factor delivery from engineered periostea is limited by poorly characterized growth factor identity, dose, and temporal availability necessary to coordinate healing in vivo. Moreover, growth factors are susceptible to degradation and their release is challenging to control, altogether demanding delivery of supraphysiologic doses that may lead to off-target pathway activation.[27, 28] Hence, growth factor delivery results in highly variable regenerative outcomes inferior to autograft healing.[19–21] While cell transplantation is also a common approach, it too has resulted in negligible improvements in graft healing, possibly due to insufficient engineered extracellular matrix (ECM) design that focuses on exogenous cell survival rather than host tissue recruitment and integration.[22–26]

To emulate autograft healing within the context of decellularized bone allografts, our lab has pioneered the tissue engineered periosteum (TEP) based on poly(ethylene glycol) (PEG) hydrogels.[29] PEG-based hydrogels are attractive engineered ECMs for bone

Author Manuscript Author Manuscript Author Manuscript Author Manuscript

regeneration[30–33] as they are biocompatible, exhibit water contents similar to many soft tissues, are resistance to nonspecific protein absorption, and are highly tunable biomechanically to match target tissue properties.[6, 34] Furthermore, the flexible chemistries used to form PEG hydrogels are amenable to incorporation of cell adhesive and/or growth factor epitopes[35, 36] as well as hydrolytically or enzymatically-tunable degradation kinetics[37]. Our previous studies[29] exploited TEP comprised of hydrolytically-degradable, tri-block copolymers (methacrylate-poly(lactide)-b-PEG-b-poly(lactide)-methacrylate, PEG-PLA-DM) functionalized with the fibronectin mimetic adhesive peptide, RGDS. Mouse mesenchymal stem cells (mMSCs) and OPs differentiated from mMSCs (mMSC-OPs) were entrapped within the TEP to emulate native periosteum cell populations and subsequent paracrine factor production.[29] mMSCs and mMSC-OPs within the TEP secreted autograft-matched osteogenic (BMP2) and angiogenic (vascular endothelial growth factor (VEGF) and Angiopoietin 1 (ANG 1)) paracrine factors which are important for endothelial cell migration and vessel formation[38–42] associated with bone callus formation and remodeling[42–44]. Despite the robust angiogenic factor production, the Hydro-TEP showed only modest increases in vascular volume compared to unmodified allograft controls.[29] Additionally, the Hydro-TEP modified allografts exhibited ~1.5 and 2-fold increases in bone callus formation and maximum torque versus unmodified allografts, respectively, at 9 weeks post-surgery. However, the maximum torque of Hydro-TEP modified allografts was only ~40% of autografts, indicating delayed healing.[29]

To augment healing mediated by the TEP, the degradation mechanism of the PEG hydrogel was investigated. Specifically, we compared Hydro-TEP, which degrades via bulk processes, with PEG hydrogels crosslinked with a MMP degradable peptide sequence, GPQGIWGQ, to enable cell-dictated degradation. Importantly, GPQGIWGQ has susceptibility to MMP2,[45, 46] MMP9,[46] and MMP14.[47] In bone regeneration, MSCs and endothelial cells (ECs) secrete MMP-2 and 9 critical for angiogenesis and tissue regeneration[48–50]. MMP-14 (MT1-MMP) is also required for ECs to cleave extracellular matrix (ECM) to generate space for lumen formation[51] while MMP-2 and 9 are necessary to degrade ECM and enable axonal outgrowth and pathfindingof neural cells[52, 53]. The ability of the MMP-degradable hydrogels to support endothelial cell migration was first tested *in vitro* using endothelial cell migration assays prior to *in vivo* experiments. As angiogenesis and innervation synergistically cooperate in bone regeneration[54], early stage neurovascularization within the TEP was assessed using immunostaining. Healing of MMP-TEP-modified allografts was evaluated versus unmodified allografts, Hydro-TEP-modified allografts, and autograft positive controls. Vascularization, bone callus formation, and tissue quality was also quantified histologically. Finally, biomechanical restoration of grafted femurs via TEP-coordinated healing was assessed via measurement of maximum torque.

2. Materials and Methods

2.1 Synthesis of PEG macromolecular monomers

2.1.1. Synthesis of PEG-PLA-DM—Linear poly(ethylene glycol) (PEG, MW 10 kDa, Alfa Aesar) was functionalized with D,L-lactide using microwave-assisted methacrylation, as previous reported[6]. The number of lactide units and methacrylate functionality (> 95%)

Author Manuscript Author Manuscript Author Manuscript Author Manuscript

per PEG macromer was analyzed by ^{1}H NMR (Bruker Avance 400 MHz, $CDCl_3$): (PEG repeat unit, -CH_2CH_2O-, 908, ~3.6 ppm; PLA repeat unit, -OC*H*(CH_3)COO-, 4H/PLA at ~5.3 ppm, and OCH(C*H*$_3$)COO-, 12H/PLA at ~1.5 ppm; C*H*$_2$=C(CH_3), 4H/macromer at ~ 5.6 and 6.3 ppm, and CH_2=C(C*H*$_3$)-), 6H/macromer at ~ 1.9 ppm.

2.1.2. Synthesis of acrylate-PEG-RGDS—The cell adhesive peptide RGDS (Arg-Gly-Asp-Ser; 433.3 Da, BACHEM Bioscience Inc., King of Prussia, PA, USA) and acrylate-PEG-N-Hydroxysuccinimide (Acrylate-PEG-SVA, 3400 Da, Laysen Bio, Arab, AL, USA) was dissolved in dimethyl sulfoxide (DMSO), then a drop of N, N-Diisopropylethylamine (DIEA) was added to the solution. The reaction was stirred overnight and then the product, acrylate-PEG-RGDS, was dialyzed against deionized water (molecular weight cutoff = 1000 Da, Spectrum Labs, Rancho Dominguez, CA, USA) and then lyophilized. Matrix-assisted laser desorption/ionization-time of flight mass spectrometry (MALDI-TOF, Bruker AutoFlex III SmartBeam, solvent: 50% acetonitrile in H_2O + 0.1% TFA; matrix: a-cyano-4-hydroxycinnamic acid (TCI Europe); calibrant: Peptide Calibration Standard (Bruker, #206195)) was used to analyzed the product (*m/z Cl*-, 3854 Da).

2.2. Synthesis of 8-arm poly(ethylene glycol) (PEG)-Norbornene (PEG-NB)

The norbornene functionalization of 8-arm PEG was achieved through *N, N'*-dicyclohexylcarbodiimide (DCC, Sigma, MO USA) coupling as previously described.[55, 56] Briefly, in one flask, 20 g of 8-arm 20 kDa PEG (Jenkem Technology, China), pyridine (5 mol for 1 mol PEG-OH, Sigma) and 4-dimethylaminopyridine (DMAP, Fisher Scientific) (0.5 mol for 1 mol PEG-OH) were dissolved in 25 mL dichloromethane (DCM, Sigma, MO, USA) for 30 min. In a second flask, DCC (5 mol for 1 mol PEG-OH) and norbornene-2-carboxylate (10 mol for 1 mol PEG-OH, Alfa Aescar, MA, USA) were dissolve in 100 mL DCM with stirring for 30 min. Solutions were combined and allowed to stir overnight. The resulting solution was vacuum filtered to remove the solid salt precipitate. Finally, PEG-norbornene was precipitated in cold diethyl ether, dissolved in 75 mL DCM, and precipitated anther two times in cold diethyl ether. The polymer was dialyzed for three days against deionized water (1000 MWCO dialysis tubing, Spectrum Laboratories) and lyophilized prior to storage at −20 °C. The structure and functionalization ratio (89%) of the 8-arm PEG-NB were determined by ^{1}H-NMR [$CDCl_3$]: δ= ~3.6 indicates PEG ether protons, δ= 5.9–6.3 indicate norbornene vinyl protons.

2.3. Peptide synthesis

The MMP-degradable crosslinker GKKCGPQGIWGQCKKG and cell adhesive ligand CGRGDSG (RGD) were synthesized on Fmoc-Gly-Wang resin (EMD) using a Liberty 1 automated peptide synthesizer with UV monitoring (CEM), as previously described[56, 57]. Amino acids were dissolved at 0.2 M in N,N-Dimethylformamide (DMF, Fisher Scientific, NH, USA). 10 wt% piperazine (Alfa Aesar) in DMF with 10 vol% ethanol was used for deprotection. 0.5 M N'-Diisopropylcarbodiimide (DIC) in DMF was used as activator, and 10 wt% Ethyl cyano(hydroxyimino)acetate (Oxyma Pure, Sigma) in DMF was used as activator base. A cleavage cocktail containing 92.5 vol% trifluoroacetic acid (TFA, Alfa Aesar), 2.5 vol% each triisopropylsilane (Alfa Aesar), 3,6-dioxa-1,8-octanedithiol (Alfa Aesar), distilled, deionized water (ddH_2O) and thioanisol (Alfa Aesar, only for peptides

Author Manuscript Author Manuscript Author Manuscript Author Manuscript

containing Arginine (R)) was used to cleavage peptides from resin for 2 h (4 h for peptides containing R). After cleavage, the peptide was precipitated in ice cold diethyl ether. Resin was removed by vacuum filtration, and peptides were collected by centrifugation. MALDI-ToF was used to verify peptide molecular weight. To verify the concentration of MMP-degradable crosslinker in solution for hydrogel synthesis, the MMP-degradable crosslinker was dissolved in ddH_2O and peptide concentration was determined via absorbance at 205 nm measured on an EvolutionTM UV-Vis detector (Thermo Scientific) as previously described[56].

2.4. Hydrogel characterization

To characterize hydrogel mechanical properties, 10 wt% PEG-NB, MMP-degradable crosslinker at a 0.6:1 thiol-ene ratio (12 mM), and 2 mM RGD were dissolved in phosphate buffered saline (PBS). 0.05 wt% lithium phenyl-2,4,6-trimethylbenzoylphosphinate (LAP), synthesized as previously described[58], was then added to the hydrogel precursor solution. Cylindrical hydrogels (diameter ~6 mm, height ~2 mm,) were fabricated via photopolymerization of 40 μL precursor solution under UV light (UVP Blak-Ray™ UV Benchtop Lamps, 365 nm, which was verified to deliver 5 mW/cm^2 at 365 nm via a UVP UVX Radiometer) for 10 minutes. After incubation in PBS overnight, the compressive moduli of the hydrogels were determined using a MTS TestWork 4® (MTS System Corporation, MN, USA) with a 5 N load cell while compressing at a rate of 0.1 mm/s at up to 10% strain[59]. The mesh size of the hydrogel was measured based on Flory-Rehner equation[59]. To perform the mesh size calculation, the volumetric swelling ratio (Q) is first calculated from equation 1:

$$Q = 1 + \frac{\rho_s}{\rho_p}\left(\frac{M_s}{M_D} - 1\right) \quad \text{Eq. 1}$$

where ρ_s is density of water (1 g/ml), ρ_p is density of PEG (1.12 g/ml), M_s and M_D are dry and wet mass of the hydrogel respectively. The molecular weight between crosslinks (M_c, in g/mol) is then calculated from equation 2:

$$\frac{1}{M_C} = \frac{2}{M_N} - \frac{\frac{\bar{V}}{V_1}(ln(1 - V_{2)} + V_2 + X_1 V_2^2)}{V_2^{\frac{1}{3}} - \frac{V_2}{2}} \quad \text{Eq. 2}$$

where M_N is the number-average molecular weight (MW) of PEG (20,000 g/mol), $\bar{V}$ is the specific volume of the polymer $\left(\bar{V} = \frac{\rho_s}{\rho_p}\right)$, V_1 is the molar volume of water (18 ml/mol), V_2 is the equilibrium polymer volume fraction of the hydrogel $\left(V_2 = \frac{1}{Q}\right)$, and X_1 is the polymer-solvent interaction parameter for PEG and water (0.426). The number of bonds between crosslinks (n) is then calculated from equation 3:

$$n = N_b \frac{M_c}{M_r} \quad \text{Eq. 3}$$

Author Manuscript Author Manuscript Author Manuscript Author Manuscript

where N_b is the number of bonds in the PEG repeat and M_r is the MW of the PEG repeat unit (44 g/mol). This allows the root-mean-square end-to-end distance of the polymer chain $\left(r_0^2\right)^{1/2}$ in nm) to be calculated from equation 4:

$$\left(r_0^2\right)^{\frac{1}{2}} = IC_n^{\frac{1}{2}} n^{\frac{1}{2}} \quad \text{Eq. 4<}$$

where I is the average bond length (0.146 nm, calculated based on C-C and C-O bond lengths) and C_n is the characteristic ratio of the polymer (4.0 for PEG). The mesh size of the hydrogel (ε) can be calculated from equation 5:

$$\varepsilon = V_2^{-\frac{1}{3}} \left(r_0^2\right)^{\frac{1}{2}} \quad \text{Eq. 5}$$

2.5. Endothelial cell sprouting in hydrogels

The ability of hydrolytically-degradable and MMP-degradable hydrogels to support endothelial cell infiltration was evaluated with a 3D co-culture spheroid sprouting assay.[60] Since the elongation and maturation of blood vessels is associated with mural cells, *i.e.* vascular smooth muscle cells (VSMCs) or pericytes[60–62], human MSCs (hMSCs), as pericyte-like cells[63], were used in this study. hMSCs isolated from bone marrow aspirates obtained from Lonza as previously described[64] were expanded in Low Glucose DMEM (Dulbecco's Modified Eagle Medium, ThermoFisher) with 10% Fetal Bovine Serum (FBS), and 1% antibiotic-antimycotic (Gibco). Human umbilical endothelial cells (HUVECs, Lonza, GA, USA) were cultured and maintained in endothelial growth media (Medium 200, Low Serum Growth Supplement (LSGS), 1% antibiotic-antimycotic, and 2% FBS, Gibco). Prior to spheroid formation, hMSCs and HUVECs were labeled with 10 μM CellTracker™ Orange (C34551, Thermo Fisher) and CellTracker™ DeepRed (C34565, ThermoFisher) respectively. hMSCs and HUVECs in a 1:1 ratio were then suspended in endothelial growth media containing 0.24 wt% methyl cellulose (M0512, Sigma) in untreated round bottomed 96-well plates to allow spheroid formation (~3000 total cells/spheroid/well)[60]. After overnight incubation at 37 °C and 5% CO_2, media was aspirated and individual spheroids were resuspended in 40 μL of either hydrolytically-degradable (10 wt% PEG-PLA-DM, 2 mM Acrylate-PEG-RGDS, 0.05 wt% LAP in PBS) or MMP-degradable (10 wt% 8-arm PEG-NB, 12 mM MMP-degradable crosslinker, 2 mM CRGDSG, 0.05 wt% LAP in PBS) hydrogel precursor solutions. Hydrogels were polymerized within cylindrical molds (diameter ~6 mm) with UV light (365 nm light at 5 mW/cm^2) for 10 minutes. The spheroid/gel systems were incubated in endothelial growth media (including 2 ng/mL VEGF and 4 ng/mL FGF), where 50 μM Marimastat[65–67] (Tocris Bioscience, MN US), a broad spectrum inhibitor of MMPs (MMP-1, 2, 7, 9, and 14), was added to the media as a control to verify MMP-specific degradation. Spheroid/gel systems were monitored using brightfield (Motic AE20) and confocal microscopy (Dragonfly Spinning Disc Confocal Microscope, Oxford Instruments Andor, CT, US). ImageJ was used to quantify endothelial cell sprouting.

Author Manuscript Author Manuscript Author Manuscript Author Manuscript

2.6. Cell culture

2.6.1. mMSC isolation—All animal experiments were approved by the University Committee on Animal Resources at the University of Rochester and complied with the National Institutes of Health guide for the care and use of Laboratory animals. Bone marrow cells were isolated from 10–14 week old C57BL6/J mice (The Jackson Laboratory, ME, USA) as previously described.[68] Mice were sacrificed and both femurs and tibias were dissected. Bone marrow was flushed out using MSC culture media (Low Glucose DMEM with 10% FBS, and 1% antibiotic-antimycotic). Cells were filtered through a 70 μm cell strainer (Fisher Scientific), and then collected by centrifugation at 1000 RPM, 4 °C, for 10 min. The collected cells were resuspended in 10 mL MSC culture media (200,00 cells/mL) and plated at cell culture dish (100 × 17 mm, ThermoFisher). When cells achieved about 60% confluence, they were detached using a cell scraper and transferred to 6-well plates (~ 0.4×10^6 cells/cm^2) for characterization and differentiation. mMSCs were characterized for putative mesenchymal stem cell markers (positive markers: CD44, CD51 and Sca-1; negative markers: CD45 and CD11b).[69, 70] Data demonstrated that ~90%, ~86% and ~95% of mMSCs were positive for CD51, Sca-1, and CD44 respectively, ~84% of mMSCs were positive for all the three stem markers, and <8% mMSCs were positive for CD45 and CD11b (Supplemental Fig. 3).

2.6.2. Osteogenic differentiation of mMSCs—Passage 1 mMSCs were differentiated into osteoprogenitors (mMSC-OPs) using osteogenic induction media Low-glucose DMEM with 10% FBS, 1% antibiotic-antimycotic, 50 μg/mL ascorbic acid and 10 mM β- glycerophosphate) for 10 days. Osteogenic differentiation was confirmed by gene expression of housekeeping gene (beta-2-microglobulin (B2M)[71, 72]) and osteogenic markers Alkaline phosphatase (ALP) and Osteocalcin (OCN) using reverse-transcription polymerase chain reaction (RT-PCR)[73, 74], and ALP staining using the 1-Step™ NBT/BCIP Substrate Solution (ThermoFisher)[75]. mMSC cultured under osteogenic conditions for 10 days (mMSC-OPs) demonstrated significantly higher ALP expression (Supplement Fig. 3A). In addition, mMSC-OPs exhibited a 3 and 5-fold increase in expression of ALP and OCN compared to undifferentiated mMSCs (Supplemental Fig. 2B and C).

2.7. TEP-modified allograft fabrication

2.7.1. Preparation of decellularized allografts—Allografts were produced from femurs dissected from BALB/c mice (The Jackson Laboratory). The method utilized in this study to prepare allografts was adapted from previous studies[11, 76–79], whereby femurs were decellularized by flushing bone marrow with PBS and thorough removal of periosteal tissue using gauze and scraping. Allografts were cut into 4 mm segments, sterilized in 70% ethanol for 30 min, rinsed in PBS, stored at −80 °C for several hours, and then transferred to −20 °C until use.

2.7.2. TEP formation—For Hydro-TEP fabrication, 10 wt% PEG-PLA-DM and 2 mM Acrylate-PEG-RGDS were dissovled in PBS. mMSCs and mMSC-OPs (at 1:1 ratio) were then suspended in the hydrogel precusor solution at a final concentration of 25×10^6 cells/mL (Fig. 1A). This cell concentration is comparable to the periosteal cell density at early stages of autograft healing.[29] For MMP-TEP fabrication, hydrogel precursor solutions were

Author Manuscript Author Manuscript Author Manuscript Author Manuscript

prepared by dissolving 2.5 mM 8-arm PEG-norbornene, 12 mM MMP-degradable crosslinker, and 2 mM CRGDSG in PBS with mMSCs and mMSC-OPs (at 1:1 ratio) suspended within the hydrogel precursor solution at 25×10^6 cells/mL (Fig. 1B). The photo-initiator LAP was then added to each cell/hydrogel solution at a final concentration of 0.05 wt%. 20 μL of PEG/cell solution was pipetted around each allograft within a custom cylindrical mold, which was subsequently exposed to 365 nm light at 5 mW/cm^2 for 10 minutes to form the TEP-allograft.[29]

2.8. Graft transplantation

A murine segmental femoral graft model was used to assess *in vivo* bone graft healing as previously described.[11, 76, 80] Mice were injected with sustained-release buprenorphine 1 hour before surgery. An 8–10 week old C57BL/6 mouse was anesthetized via isoflurane (M3000 Table Top, Non-Rebreathing Anesthesia Machine, SUPERA, Clackamas, OR, USA). An 8 mm-long incision was made, and the mid-shaft of the femur was exposed via blunt dissection. The femoral defect was made by using a Dremel with double diamond blades (with 4 mm spacing). An autograft, unmodified allograft, Hydro-TEP-modified allograft, or MMP-TEP-modified allograft was transplanted into the defect and stabilized with 25-gauge spinal needles (VWR, PA, USA). For autografts, dissected segments were flipped and immediately transplanted back into the same mouse. After placement, the skeletal muscle and skin were sutured. After surgery, mice were allowed to mobilize without restriction.

2.9. Assessment of graft healing *in vivo*

2.9.1. Micro-perfusion and quantification of vascularization via micro-computed tomography (μCT)—

At 3, 6, and 9 weeks after implantation, a radiopaque lead chromate silicon rubber contrast agent (MicrofilMV-122, Flow Tech; Carver, MA,USA) was perfused into mice[29]. Grafted femurs were dissected after perfusion and scanned using μCT (Explore; GE HealthCare) to image both blood vessels and bone tissue. Subsequently, femur samples were decalcified in 14% ethylenediaminetetraacetic acid (EDTA) for 14 days and scanned again to image the remaining vessels. Graft vascularization was quantified using μCT images volumes of interest (VOI) before and after decalcification.

2.9.2. Bone callus volume quantification via μCT—

The μCT system was used to analyze bone callus formation. Consistent VOI were selected for two-dimensional (2D) images reconstruction with the same threshold. Both host cortical bone and transplanted graft were included in the contour lines during the measurement of new bone callus volume. New bone callus volume in a VOI spanning the entire length of the transplanted bone graft and 1 mm of the proximal and distal host cortical bone was used to evaluate graft healing.

2.9.3. Histological staining and histomorphometric analysis—

At 3, 6, and 9 weeks post-surgery, grafted femurs were harvested, and fixed in 4% neutral buffered formalin (NBF) for 72 hours, washed with PBS, and then decalcified in 14% EDTA for two weeks. Decalcified samples were horizontally embedded in paraffin and then sectioned at 5 μm from three nonconsecutive levels. Tissues were stained with Alcian Blue (pH 2.4) (blue, glycosaminoglycans/proteoglycans) and Orange G (pink, bone/soft tissue). Stained sections

Author Manuscript Author Manuscript Author Manuscript Author Manuscript

were scanned by Olympus VS110 Virtual Microscopy System. Subsequently, Visiopharm® was used to perform the histomorphometric analysis, wherein mesenchyme, cartilage, and woven bone area were reported based on color threshold intensities[81]. Visiopharm® was used to perform the histomorphometric analysis of high resolution images, such as those in Figure 6, wherein mesenchyme, cartilage, and woven bone area were reported based on color threshold intensities[81, 82]. The histomorphometric algorithm was development based on a previous study[82]. First, newly formed woven bone, cartilage, and mesenchymal tissues are assigned to different colors via manual selection. As more areas of the tissue type are sampled, the program "learns" the range of colors within that tissue. The same color assignments for tissues were used for all samples. Then, regions of interest (ROI) were defined and the program automatically measures tissue area.

2.9.4. Immunohistochemical staining and analysis—3 weeks post-surgery tissues were embedded in paraffin vertically and 5 μm sections were obtained at three nonconsecutive levels proximal, medial, and distal to the allograft region to capture cross sections spanning the graft callus area (Supplemental Fig. 1). To qualitatively analyze neurovascularization during early-stage graft healing, sections were immunostained for CD31 (platelet endothelial cell adhesion molecule; PECAM), an endothelial marker[83, 84], and beta tubulin III (β3-tubulin), a neuronal marker which has previously been associated with neurogenesis[85]. Briefly, slides were deparaffinized and heat induced antigen retrieval was performed using Tris-EDTA buffer (pH = 9). Sections were blocked with 10% normal goat serum (NGS) for 1 hour then incubated with rabbit polyclonal CD31 antibody (1:200 dilution, ab28364, Abcam) in PBSA (bovine serum albumin (BSA, heat shock fraction, powder, Sigma) in PBS (0.1% (w/v)) buffer overnight at 4 °C. After washing with PBS, slides were incubated in goat anti-rabbit secondary antibody (1;500 dilution, A-21245, ThermoFisher) for 1 hour. A second block with 10% normal rabbit serum was performed for 30 min at room temperature, and sections were washed in PBS for 1 hour and stained with unconjugated goat anti-rabbit Fab-fragment (dilution to 30 μg/mL in 0.1% PBSA, Jackson ImmunoResearch, PA, USA) for 1 h at room temperature. Followed by the second primary antibody β3-Tubulin (1:200 dilution in 0.1% PBSA, Ab18207, Abcam). Subsequently, slides were incubated with the second secondary antibody (1:500 dilution in 0.1% PBSA, F2765, ThermoFisher). After wash in PBS, slides were incubated with DAPI (1:500 dilution, ThermoFisher) for 5 min then TrueBlack (1:20 dilution in 70% ethanol, Biotium, CA, US) for 5 min. After a final wash with PBS, slides were mounted using Immu-Mount™ (ThermoFisher) and imaged using a Dragonfly Spinning Disc Confocal Microscope (Oxford Instruments Andor, CT, US). ImageJ was used to quantify the vessel and nerve densities and identify colocalization.

To evaluate endochondral ossification at early stages of graft healing to correlate with histology analysis, two serial sections of the same tissue used for histology at 3 weeks post-surgery were immunostained for Col2a1 and Col10a1. Briefly, slides were deparaffinized and antigen retrieval was performed at 37 °C using 0.01 M HCl with 4 mg/ml of pepsin for 10 min. Sections were blocked with 10% NGS for 30 min then incubated with Col2a1 (mouse monoclonal primary antibody, 1:100 dilution, MS235, ThermoFisher) or Col10a1 (mouse polyclonal primary antibody, 1:500 dilution, Quartett antibody, # 2031501005)

Author Manuscript Author Manuscript Author Manuscript Author Manuscript

overnight at 4 °C. After washing with PBS, slides were incubated in goat anti-mouse secondary antibody (Alexa Fluor 488, A-11001, ThermoFisher) for 1 hour at room temperature. After wash in PBS, slides were incubated with DAPI (1:500 dilution, ThermoFisher) for 5 min. After a final wash with PBS, slides were mounted using Immu-MountTM (ThermoFisher) and imaged using a Dragonfly Spinning Disc Confocal Microscope (Oxford Instruments Andor, CT, US).

2.9.5. Assessment of graft torsional biomechanics—Grafted femurs along with the contralateral intact femur were harvested after 6 and 9 weeks. Proximal and distal femur ends were cemented into an aluminum tube using a custom jig to ensure axial alignment and maintain a gauge length of 6 mm for all samples. Samples were mounted on an EnduraTec TestBench system (200 N·mm torque cell; Bose Corp., Minnetonka, MN) and tested in torsion at a rate of 1°/sec until failure to determine maximum torque.[6, 29]

2.10. Rationale for using previous data set

In an effort to significantly reduce the use of animals in this study[86, 87], graft healing data, including vascularization, bone callus formation, histology, and biomechanical analyses of autografts, allografts, and Hydro-TEP modified allografts at 6 and 9 weeks post-surgery are derived from the same data set of our previous published study[29], as experimental methods and animal strains did not differ from the current investigation. However, different representative images are shown herein[29]. Additionally, alternative data analysis approaches were performed to yield additional insight for this study. For example, vascularization VOI was chosen to be within the graft area instead of the entire tissue volume, as previously published[29]. Additionally, maximum torque strengths were normalized to intact femurs to better reflect the extent of healing versus unaltered controls.

2.11. Statistical analysis

Raw data was plotted in GraphPad Prism Software and shown in figures as mean ± standard deviation. Replicate number of samples were determined based on previous data[6, 29] using power analysis[88]. GraphPad Prism software was also applied for statistical analysis of data, where one-way or two-way ANOVA with Dunnett's and Tukey's post-hoc testing analysis respectively, as noted in figure legends, was used identifying significant differences with $p < 0.05$ considered statistically significant.

3. Results

3.1. Endothelial cell migration into hydrogels

To test the hypothesis that MMP-degradable hydrogels support endothelial cell migration, HUVEC/hMSC spheroids were encapsulated into either hydrolytically degradable (Hydro Gel) or MMP-degradable (MMP Gel) hydrogels with MMP inhibitor as a control. Migration distances from the spheroids were measured after 1, 3, and 5 days of culture to determine if the mode of hydrogel degradation affected endothelial migration. Note that neither bulk hydrogel modulus nor mesh size differed between Hydro and MMP gels (Supplemental Fig. 2), which ensures that cell behaviors were only impacted by degradation mechanism and not initial hydrogel mechanical properties. Additionally, spheroids encapsulated in gels were

Author Manuscript Author Manuscript Author Manuscript Author Manuscript

verified to have similar sizes (Supplemental Fig. 3). Confocal microscopy images (Fig. 2B) illustrate that HUVECs (in yellow) and hMSCs (in red) concomitantly (orange) migrated into the MMP Gels, indicative of endothelial cell migration. Specifically, within the MMP Gel group, cell migration lengths of 118 ± 17 μm were observed after 3 days which reached 347.6 ± 20.1 μm at day 5 (Fig. 2 C–E). Very limited cell sprouting can be observed when MMP inhibitor was added in the media (Fig. 2B and E), indicating the degradation of the MMP-Gel is MMP-mediated. In contrast, no cell migration was observed even at day 5 (Fig. 2 C and D) in the hydrolytically degradable gel, which supports the hypothesis that the rate and/or mechanism of hydrolytic gel degradation does not support endothelial cell migration and may inhibit host tissue infiltration during healing.

3.2. Early-stage neurovascularization of autografts, allografts, and TEP-modified allografts *in vivo*

The MMP-degradable hydrogel was shown to support EC migration *in vitro* (Fig. 2), which may support host tissue infiltration *in vivo*[89, 90]. To test this hypothesis, MMP-degradable hydrogel precursors with mMSCs and mMSC-OPs were photopolymerized under UV around allografts to form the MMP-TEP modified allograft, which was then implanted into a critically-sized murine femur defect. Angiogenesis, the sprouting of new capillaries from existing blood vessels[91], is activated by hypoxic stress immediately following injury, and is critical for healing in bone and other tissues[92]. Angiogenesis and innervation are anatomically coupled in bone tissue and synergistically coordinate bone regeneration.[93, 94] Therefore, it is important to evaluate if early-stage neurovascularization is coordinated by the TEP. Compared to unmodified and Hydro-TEP-modified allografts, the MMP-TEP supported significantly increased blood vessel and nerve densities at all three levels (Supplemental Fig. 1) after 3 weeks, which was comparable to the vessel and nerve density observed in autografts (Fig. 3B and C). Positive staining of CD31 and β3-tubulin at all 3 levels measured (Supplemental Fig. 1) within the graft callus indicated successful host vascular infiltration and innervation, respectively. Additionally, co-localization of vessels and nerves was observed for both autografts and MMP-TEP-modified allografts (Fig. 3A, white arrows), while co-localization was not observed within either unmodified allografts or Hydro-TEP-modified allografts (Fig. 3A). These findings indicate that the MMP-TEP promotes early-stage neurovascularization, which, in turn, may improve overall healing.

3.3. Graft-localized vascularization of autografts, allografts, and TEP-modified allografts *in vivo*

In addition to staining to detect early-stage neurovascularization, μCT analysis was used to longitudinally evaluate graft-localized vascularization. μCT images demonstrated extensive vascularization for both autografts and MMP-TEP-modified allografts at 3, 6, and 9 weeks post implantation, with the entire graft area completely infiltrated by blood vessels at 9 weeks post-implantation in both groups (Fig. 4A). In contrast, both unmodified and Hydro-TEP-modified allografts showed few blood vessels in the callus and graft area even after 6 and 9 weeks (Fig. 4A). At 3 and 6 weeks post-implantation, the graft-localized vascular volume of MMP-TEP-modified allografts (0.216 ± 0.77 mm^3 and 0.20 ± 0.076 mm^3) was significantly greater than that of allografts (0.002 ± 0.0004 mm^3 and 0.053 ± 0.048 mm^3) and Hydro-TEP-modified allografts (0.056 ± 0.004 mm^3 and 0.023 ± 0.015 mm^3) (Fig. 4B).

Author Manuscript Author Manuscript Author Manuscript Author Manuscript

At 9 weeks post-implantation, the graft-localized vascular volume for Hydro-TEP-modified allografts (0.045 ± 0.019 mm^3) was significantly lower than that of autografts (0.22 ± 0.112 mm^3) and of MMP-TEP-modified allografts (0.09 ± 0.067 mm^3), with no significant difference between the latter two groups. These data indicate that the MMP-TEP improved graft-localized vascularization during allograft healing.

3.4. Bone callus formation of autograft, allograft, and TEP-modified allografts *in vivo*

Bone callus volume and mineralization, important indicators of graft healing, were quantified for autografts, allografts, and Hydro/MMP-TEP-modified allografts at 3, 6, and 9 weeks post-surgery (Fig. 5). In agreement with previous studies[11, 29, 95, 96], bridging callus (volume of 4.6 ± 0.6 mm^3) was observed in autografts by 3 weeks, with subsequent graft and callus resorption and remodeling at 6 (3.5 ± 0.6 mm^3) and 9 weeks (2.6 ± 0.9 mm^3) (Fig. 5A and B), resulting in reduced vascular volume (Figure 4B) to that of naïve bone (Figure 5B) (6). On the contrary, only modest callus formation was observed in unmodified allograft-treated defects, which was limited to proximal and distal sites of the graft after 3 weeks (1.3 ± 0.2 mm^3) with no sign of callus bridging even after 6 (1.4 ± 0.2 mm^3) and 9 weeks (2.0 ± 0.4 mm^3) (Fig. 5A and B). Compared to allografts, both Hydro-TEP and MMP-TEP supported significantly enhanced bone callus volume (Fig. 5B). Hydro-TEP-modified allografts exhibited 3.5 (4.6 ± 0.5 mm^3), 3.6 (5.0 ± 0.8 mm^3), and 2.9-fold (5.7 ± 1.6 mm^3) increases in average bone volume versus unmodified allografts at 3, 6, and 9 weeks post-implantation, respectively (Fig 5B). MMP-TEP-modified allografts showed 4.5 (5.8 ± 1.4 mm^3), 4.6 (6.5 ± 1.9 mm^3), and 2.8-fold (5.6 ± 1.6 mm^3) higher average bone volume versus unmodified allografts at 3, 6, and 9 weeks post-implantation, respectively (Fig. 5B). There were no significant differences in bone callus volume between Hydro-TEP and MMP-TEP-modified allografts at any point. However, since endochondral callus formation is reflected by the volume, shape, and mineralization of the callus, robust bone regeneration cannot be determined only through bone callus volume[97, 98]. Rather, mineralized callus that bridges the defect is necessary for bone healing and ultimate restoration of bone biomechanics[99]. Bridging callus of MMP-TEP can be observed both proximally and distally from week 3 to week 9 (Figure 5A) with higher mineralization (987.7 ± 48.7 mg HA/ccm) versus Hydro-TEP-modified allografts (810.1 ± 201.7 mg HA/ccm) (Figure 5C), while very limited bridging callus can be observed for unmodified and Hydro-TEP-modified allografts even after 9 weeks (Figure 5A). Taken together, these data demonstrate MMP-TEP enhanced bridging callus formation and mineralization in comparison to unmodified allografts versus and Hydro-TEP functionalized allografts.

At 3, 6, and 9 weeks post-implantation, histological analysis of grafted femurs was performed using Alcian blue and Orange G staining. Consistent with the μCT results (Fig. 5), autografts were almost completely bridged by newly formed bone (orange arrow) with minimal cartilage (black arrow) after 3 weeks (Fig. 6A). Graft and callus remodeling was observed after 6 and 9 weeks (Fig. 6A), where hard and total callus areas were significantly decreased after week 6 (Fig. 6B ii and vi respectively). In contrast, minimal soft (black arrow) and hard (orange arrow) callus had formed at the proximal and distal ends of unmodified allografts with obvious fibrotic tissue (green arrow) at 3 weeks post-surgery (Fig. 6A). Similarly, after 6 and 9 weeks, unmodified allografts had limited hard and total

Author Manuscript Author Manuscript Author Manuscript Author Manuscript

callus area (Fig. 6A, B ii and vi). Histology revealed that Hydro-TEP modified allografts exhibited minimal hard callus formation and significant fibrotic tissue (Fig. 6A, green arrow) at 3 weeks post-implantation at levels comparable to unmodified allografts (Fig. 6B ii). Despite an increased hard callus area for Hydro-TEP modified allografts at weeks 6 and 9 (Fig. 6B), modest bridging callus (orange arrow) was observed along with the presence of considerable fibrotic tissue (green arrow) (Fig. 6A). After 3 weeks, produce of Col II and X can be observed in the MMP-TEP group, indicating the advanced endochondral ossification, while only produce of Col II can be observed in allograft and Hydro-TEP groups, indicating immature ossification[100]. Moreover, the hard callus (orange arrow) had begun to bridge from both ends of the graft at 3 weeks post-surgery (Fig. 6A), exhibiting significantly increased hard callus area (2.04 ± 0.61 mm^2) relative to unmodified allografts (0.71 ± 0.17 mm^2) (Fig. 6B ii). After 6 and 9 weeks, MMP-TEP-modified allografts displayed extensive bridging callus (orange arrow, Fig. 6A) with areas (3.42 ± 1.39 mm^2, 2.23 ± 0.41 mm^2) comparable to those of autografts (3.66 ± 1.1 mm^2, 2.67 ± 0.63 mm^2) (Fig. 6B) at 6 and 9 weeks post-implantation.

3.5. Mechanical properties of autografts, allografts, and TEP-modified allografts

As an indicator of biomechanical stability and maturation of bone during graft healing, maximal torsion strength (maximum torque) of grafted femurs was measured at 6 and 9 weeks post-implantation (Fig. 7). Maximum torques of autografts were 79% and 77% of intact femurs after 6 and 9 weeks, which was 7 and 6-times greater than those of unmodified allografts, respectively. Hydro-TEP-modified allografts exhibited only 5% and 28% of intact femur maximum torque at 6 and 9 weeks post-surgery. While Hydro-TEP showed a higher maximum torque than unmodified allografts after 9 weeks, values were still significantly lower compared to autografts. The MMP-TEP significantly increased biomechanical stability of allografts at both 6 (40.9 ± 27.8 %) and 9 (52.5 ± 29.7%) weeks post-implantation, reaching a statistically comparable maximum torque to that of autografts at 9 weeks post-surgery. Hence, the MMP-TEP significantly enhanced the biomechanical stability of femur allografts, indicating improved and more mature healing.

4. Discussion

To identify the critical cues that coordinate periosteal-mediated healing, we have pioneered the development of a TEP[29] using an engineered ECM based on PEG hydrogels that localize regenerative MSCs and OPs to the graft surface, akin to native periosteum[29]. The TEP emulates the level and cascade of periosteal angiogenic factors but only modestly increases angiogenesis and healing of allografts[29]. To investigate the hypothesis that the underlying degradation mechanisms of the engineered periosteum are critical for coordinating host tissue infiltration necessary for successful bone healing, MMP-degradable crosslinkers were incorporated within the engineered periosteal matrix to provide cell-dictated degradation, thus enabling structural support of infiltrating host tissue. In comparison to unmodified and Hydro-TEP-modified allografts, the MMP-TEP significantly promoted early stage neurovascularization within the MMP-TEP-modified allografts. Additionally, greater levels of bridging hard callus formed around MMP-TEP-modified allografts with greater mineralization density (Fig. 5 A and C) and minimal fibrous tissue

Author Manuscript Author Manuscript Author Manuscript Author Manuscript

(Fig. 6A) were observed after 6 and 9 weeks, likely due to the robust early stage neurovascularization (Fig. 3) and longitudinal graft-localized vascularization (Fig. 4) of MMP-TEP-modified allografts compared to unmodified and Hydro-TEP-modified allografts. Consequently, enhanced mineralization of bone callus (Fig. 5) lead to 4-fold, 2-fold increased maximum torques for MMP-TEP-modified allografts versus unmodified and Hydro-TEP-modified allografts after 9 weeks, respectively (Fig. 7).

The periosteum is essential for autograft healing. After injury, periosteal stem cells within the periosteum undergo robust proliferation and secrete pro-inflammatory cytokines to recruit angiogenic and regenerative cells and initiate angiogenesis.[101, 102] New capillaries sprout and inosculation occurs between the host tissue and live periosteum to provide oxygen and nutrients required for cell recruitment and proliferation, differentiation, and tissue production consistent with successful regeneration.[103, 104] In particular, type H capillaries, characterized by high expression of CD31, can direct bone regeneration by stimulating the proliferation and differentiation of osteoprogenitors recruited into the injury site[105, 106] and promote chondrocyte maturation and hypertrophy during soft callus formation[83]. Periosteal nerve regeneration is initiated by the injury in parallel with and in close proximity to the regenerating vascularization, a process coordinated by the production of chemotactic cues including nerve growth factor by Schwann cells and macrophages[107–109].

Unlike autografts, the healing of allografts cannot rely upon coordination by preexisting cells, vessels, and nerves within the collagenous periosteal matrix, which can be remodeled by infiltrating host tissues. Rather, the TEP must imbibe the critical facets of this complex niche to initiate healing. It is clear that cells transplanted within the TEP are necessary to initiate healing either directly through differentiation[110–112] or indirectly, through paracrine factor production[6, 22, 81], or some combination thereof. However, our data indicate the mechanism of TEP degradation is also a critical design parameter. Angiogenesis within hydrolytically-degradable matrices (Hydro-TEP) paled in comparison to autografts and MMP-degradable matrices (MMP-TEP) (Fig. 3 and 4). This outcome was likely due to inhibition of initial vessel recruitment within Hydro-TEP, as the mesh size (~15 nm)[29] is smaller than that of the leading filipodia of migrating cells (0.2–0.4 μm)[113] (Fig. 2C). Our previous data[114] suggest that a > 90% mass loss of PEG-PLA-DM hydrogels is required for the mesh size to approach 0.2 μm. At this point, the hydrogel would be very close to reverse gelation and, thus, would be unable to support infiltrating vessels, undermining angiogenic network stability. Even though the MMP-degradable hydrogels (MMP-Gel) have similar initial mesh size to their hydrolytically degradable counterparts (Supplemental Fig. 2B), the MMP-Gel can support EC migration (Figure. 2A, B and D) via pericellular secretion of MMPs. During angiogenesis and innervation, MMP-TEP is locally degraded by cells during endothelial cell and axonal migration and extension[51, 52]. Hence, unlike the hydrolytically degradable hydrogel, cells and axonal migration and vessel infiltration do not require bulk degradation of the MMP degradable hydrogel to attain the threshold mesh size. Along with mediating ECM remodeling, MMPs have other functional implications in angiogenesis and innervation. MMP1, 9, and 10 can regulate EC invasion and lumen formation[115, 116]. MMP9 modulates VEGF expression[117] and MMP9-deficient mice exhibit delayed angiogenesis with growth plate abnormalities in the long bones during

Author Manuscript Author Manuscript Author Manuscript Author Manuscript

skeletal development[118–120]. MMP2 and 9 have been reported to regulate axonal outgrowth and guidance.[121, 122]

Angiogenesis and innervation are coordinated processes during bone regeneration[54]. During this process, nerve fibers secrete vasculogenic neuropeptides, such as substance P (SP) and calcitonin gene-related peptide (CGRP), to stimulate angiogenesis.[93, 123] Concurrently, neuropeptides, such as CGRP[124] and vasoactive intestinal polypeptide (VIP),[125, 126] enhance the proliferation and osteogenic differentiation of MSCs and production of osteoblasts. Endothelial cells secrete artemin and neurotrophin 3 (NT-3) to recruit axons to track alongside vessels[127, 128], and Schwann cells can produce VEGF to encourage angiogenesis and track blood vessels alongside nerve fibers[129]. In accordance with these findings, *in vitro* endothelial sprouting within MMP-degradable hydrogels (Figure. 2C, D, and E) paralleled significantly enhanced vessel and nerve densities observed *in vivo* (Fig. 3B and C), along with co-localized vessels and nerves, comparable to autograft controls (Fig. 3A), and longitudinal graft-localized vascularization (Fig. 4). Endochondral callus formation and ossification are also regulated by blood vessel infiltration[17, 130] and innervation[16, 17, 93, 123]. Consequently, the robust neurovascularization of MMP-modified allografts significantly increase mineralized endochondral callus formation versus unmodified and Hydro-TEP modified allografts (Figs. 5 and 6), leading to enhanced maximum torque strengths of grafted femurs which was comparable to that of autografts at 9 weeks post-surgery (Fig. 7). In summary, these data indicate that the MMP-TEP effectively coordinates allograft healing via early stage recruitment and support of host neurovascularization.

Our findings regarding hydrogel degradation mechanism and its impact on tissue regeneration are not unique. Altering the mechanism of hydrogel degradation from hydrolytic to MMP-sensitive has been reported to promote cell proliferation and migration necessary for bone regeneration.[34, 56, 131] Indeed, MMP-degradable hydrogels effectively supported blood vessel infiltration via VEGF delivery, though this approach ultimately failed to enhance bone regeneration, likely due to reliance solely on VEGF to initiate healing.[19] Baldwin et al.[25] transplanted MSCs/HUVECs within heparin-functionalized PEG hydrogels to treat rabbit tibia defects, whereby overall vascularization and bone regeneration was improved. MMP-degradation, in particular, was suggested to support the high level of host cell infiltration and modulation of angiogenesis, osteogenesis, and healing.[25] The underlying implications of degradation mechanism does not only apply to mesenchymal tissue regeneration; MMP-degradable hydrogels enhanced salivary gland epithelial tissue apicobasolateral organization and function versus hydrolytically degradable hydrogels.[56]

Although the MMP-TEP improved allograft healing, overall outcomes still lagged behind that of autografts. Since PEG-based hydrogels offer synthetic flexibility[132–134], additional matrix cues can be explored to further improve healing. For example, additional or alternative ECM-derived peptides beyond RGD, *e.g.* GFOGER and YIGSR, can be covalently linked into hydrogel scaffolds to support specific matrix-integrin binding interactions which mediate angiogenesis and innervation during bone regeneration[135–137]. Additionally, TEP-mediated healing can be further investigated as a function of MMP-degradable crosslinker susceptibility by changing peptide sequences to alter crosslinker

Author Manuscript Author Manuscript Author Manuscript Author Manuscript

degradation rates or sensitivity to specific MMPs associated with angiogenesis and/or innervation[46, 138–140].

Conclusions

A cellularly-degradable (*i.e.* MMP-degradable) PEG hydrogel-based tissue engineered periosteum was investigated to coordinate the infiltration of critical regenerative host cells during bone allograft graft healing. As a result, early stage neurovascularization was enhanced, and hard bone callus formation was improved versus unmodified allografts via effective support of cell recruitment and migration. In comparison to unmodified allografts, the MMP-TEP supported significantly increased numbers of blood vessels and nerve densities, vessel and nerve co-localization, and graft-localized vascularization comparable to autograft-mediated healing. Additionally, a more mature hard callus formed around MMP-TEP-modified allografts versus Hydro-TEP-modified allografts. Consequently, MMP-TEP-modified allografts exhibited enhanced biomechanical stability (maximum torque) comparable to that of autografts at 9 weeks post-surgery. These results indicate the MMP-TEP successfully improved allograft healing by promoting early-stage neurovascularization. Despite improvements in allograft healing via the MMP-TEP, outcomes still fall below those from autografts. Thus, future experiments will focus on optimizing TEP matrix cue to promote more effective allograft healing.

Supplementary Material

Refer to Web version on PubMed Central for supplementary material.

Acknowledgements

This project was funded by the National Institutes of Health (NIH) (R01 AR064200, P30 AR06955) and the National Science Foundation (NSF CBET 1450987). The authors also wish to thank Matthew Ingalls for helping with the IHC co-staining protocol, Mike Thullen for μCT imaging and analysis, Emma Gira for biomechanical testing, Jeffrey Fox and Kathy Maltby for histology assistance, Dr. Tzong-Jen Sheu and Ashley Proctor for their surgical expertise and training, and David Fraser and Jared Mereness for manuscript review.

References:

1. Shegarfi H, Reikeras O. Bone transplantation and immune response. Journal of Orthopaedic Surgery. 2009;17(2):206–11. [PubMed: 19721154]
2. Kumbar S, Toti U, Deng M, James R, Laurencin C, Aravamudhan A, Harmon M, Ramos D. Novel mechanically competent polysaccharide scaffolds for bone tissue engineering. Biomedical Materials. 2011;6(6):065005. [PubMed: 22089383]
3. Meijer GJ, de Bruijn JD, Koole R, van Blitterswijk CA. Cell-based bone tissue engineering. PLoS Med. 2007;4(2):e9. [PubMed: 17311467]
4. Wang W, Yeung KW. Bone grafts and biomaterials substitutes for bone defect repair: A review. Bioactive materials. 2017;2(4):224–47. [PubMed: 29744432]
5. Zimmermann G, Moghaddam A. Allograft bone matrix versus synthetic bone graft substitutes. Injury. 2011;42:S16–S21. [PubMed: 21889142]
6. Hoffman MD, Xie C, Zhang X, Benoit DS. The effect of mesenchymal stem cells delivered via hydrogel-based tissue engineered periosteum on bone allograft healing. Biomaterials. 2013;34(35):8887–98. [PubMed: 23958029]
7. Greenwald AS, Boden SD, Goldberg VM, Khan Y, Laurencin CT, Rosier RN. Bone-graft substitutes: facts, fictions, and applications. JBJS. 2001;83:98–103.

Author Manuscript Author Manuscript Author Manuscript Author Manuscript

8. Hussein KH, Park K-M, Kang K-S, Woo H-M. Biocompatibility evaluation of tissue-engineered decellularized scaffolds for biomedical application. Mater Sci Eng C. 2016;67:766–78.

9. Malizos KN, Papatheodorou LK. The healing potential of the periosteum: molecular aspects. Injury. 2005;36(3):S13–S9. [PubMed: 16188544]

10. Colnot C Skeletal cell fate decisions within periosteum and bone marrow during bone regeneration. J Bone Miner Res. 2009;24(2):274–82. [PubMed: 18847330]

11. Zhang X, Xie C, Lin AS, Ito H, Awad H, Lieberman JR, Rubery PT, Schwarz EM, O'Keefe RJ, Guldberg RE. Periosteal progenitor cell fate in segmental cortical bone graft transplantations: implications for functional tissue engineering. J Bone Miner Res. 2005;20(12):2124–37. [PubMed: 16294266]

12. Evans SF, Chang H, Knothe Tate ML. Elucidating multiscale periosteal mechanobiology: a key to unlocking the smart properties and regenerative capacity of the periosteum? Tissue Engineering Part B: Reviews. 2013;19(2):147–59. [PubMed: 23189933]

13. Lange J, Sapozhnikova A, Lu C, Hu D, Li X, Miclau T III, Marcucio RS. Action of IL-1β during fracture healing. J Orthop Res. 2010;28(6):778–84. [PubMed: 20041490]

14. Ankrum J, Karp JM. Mesenchymal stem cell therapy: Two steps forward, one step back. Trends Mol Med. 2010;16(5):203–9. [PubMed: 20335067]

15. Diefenderfer DL, Osyczka AM, Reilly GC, Leboy PS. BMP responsiveness in human mesenchymal stem cells. Connect Tissue Res. 2003;44(1):305–11. [PubMed: 12952214]

16. Newman MR, Benoit DS. Local and targeted drug delivery for bone regeneration. Curr Opin Biotechnol. 2016;40:125–32. [PubMed: 27064433]

17. Dimitriou R, Tsiridis E, Giannoudis PV. Current concepts of molecular aspects of bone healing. Injury. 2005;36(12):1392–404. [PubMed: 16102764]

18. Granero-Moltó F, Weis JA, Miga MI, Landis B, Myers TJ, O'Rear L, Longobardi L, Jansen ED, Mortlock DP, Spagnoli A. Regenerative effects of transplanted mesenchymal stem cells in fracture healing. Stem Cells. 2009;27(8):1887–98. [PubMed: 19544445]

19. García JR, Clark AY, García AJ. Integrin-specific hydrogels functionalized with VEGF for vascularization and bone regeneration of critical-size bone defects. J Biomed Mater Res A. 2016;104(4):889–900. [PubMed: 26662727]

20. Romero R, Travers JK, Asbury E, Pennybaker A, Chubb L, Rose R, Ehrhart NP, Kipper MJ. Combined delivery of FGF-2, TGF-β1, and adipose-derived stem cells from an engineered periosteum to a critical-sized mouse femur defect. J Biomed Mater Res A. 2017;105(3):900–11. [PubMed: 27874253]

21. Wu L, Gu Y, Liu L, Tang J, Mao J, Xi K, Jiang Z, Zhou Y, Xu Y, Deng L. Hierarchical micro/nanofibrous membranes of sustained releasing VEGF for periosteal regeneration. Biomaterials. 2020;227:119555. [PubMed: 31655445]

22. Guo H, Li X, Yuan X, Ma X. Reconstruction of radial bone defects using the reinforced tissue-engineered periosteum: An experimental study on rabbit weight-bearing segment. Journal of Trauma and Acute Care Surgery. 2012;72(2):E94–E100.

23. Zhou Y, Chen F, Ho ST, Woodruff MA, Lim TM, Hutmacher DW. Combined marrow stromal cell-sheet techniques and high-strength biodegradable composite scaffolds for engineered functional bone grafts. Biomaterials. 2007;28(5):814–24. [PubMed: 17045643]

24. Shi X, Zhou J, Zhao Y, Li L, Wu H. Gradient-Regulated hydrogel for interface tissue engineering: steering simultaneous Osteo/Chondrogenesis of stem cells on a chip. Advanced healthcare materials. 2013;2(6):846–53. [PubMed: 23193109]

25. Baldwin J, Wagner F, Martine L, Holzapfel B, Theodoropoulos C, Bas O, Savi F, Werner C, De-Juan-Pardo E, Hutmacher D. Periosteum tissue engineering in an orthotopic in vivo platform. Biomaterials. 2017;121:193–204. [PubMed: 28092776]

26. Wang T, Zhai Y, Nuzzo M, Yang X, Yang Y, Zhang X. Layer-by-layer nanofiber-enabled engineering of biomimetic periosteum for bone repair and reconstruction. Biomaterials. 2018;182:279–88. [PubMed: 30142527]

27. Visser NJ, Rezaie ES, Friedrich PF, Kotsougiani D, Shin AY, Bishop AT. Effects of Surgical Angiogenesis on Segmental Bone Reconstruction With Cryopreserved Massive-Structural

Author Manuscript Author Manuscript Author Manuscript Author Manuscript

Allografts in a Porcine Tibia Model. Journal of Orthopaedic Research®. 2019;37(8):1698–708. [PubMed: 31042307]

28. Takahata M, Awad HA, O'Keefe RJ, Bukata SV, Schwarz EM. Endogenous tissue engineering: PTH therapy for skeletal repair. Cell Tissue Res. 2012;347(3):545–52. [PubMed: 21626290]
29. Hoffman MD, Benoit DS. Emulating native periosteum cell population and subsequent paracrine factor production to promote tissue engineered periosteum-mediated allograft healing. Biomaterials. 2015;52:426–40. doi: 10.1016/j.biomaterials.2015.02.064. [PubMed: 25818449]
30. Zhao X, Liu S, Yildirimer L, Zhao H, Ding R, Wang H, Cui W, Weitz D. Injectable stem cell-laden photocrosslinkable microspheres fabricated using microfluidics for rapid generation of osteogenic tissue constructs. Adv Funct Mater. 2016;26(17):2809–19.
31. Shekaran A, García JR, Clark AY, Kavanaugh TE, Lin AS, Guldberg RE, García AJ. Bone regeneration using an alpha 2 beta 1 integrin-specific hydrogel as a BMP-2 delivery vehicle. Biomaterials. 2014;35(21):5453–61. [PubMed: 24726536]
32. Dyondi D, Webster TJ, Banerjee R. A nanoparticulate injectable hydrogel as a tissue engineering scaffold for multiple growth factor delivery for bone regeneration. International journal of nanomedicine. 2013;8:47. [PubMed: 23293519]
33. Zhai X, Ma Y, Hou C, Gao F, Zhang Y, Ruan C, Pan H, Lu WW, Liu W. 3D-printed high strength bioactive supramolecular polymer/clay nanocomposite hydrogel scaffold for bone regeneration. ACS Biomaterials Science & Engineering. 2017;3(6):1109–18. [PubMed: 33429585]
34. Sokic S, Papavasiliou G. Controlled proteolytic cleavage site presentation in biomimetic PEGDA hydrogels enhances neovascularization in vitro. Tissue engineering Part A. 2012;18(23–24):2477–86. [PubMed: 22725267]
35. Elisseeff J, Puleo C, Yang F, Sharma B. Advances in skeletal tissue engineering with hydrogels. Orthodontics & craniofacial research. 2005;8(3):150–61. [PubMed: 16022717]
36. Lin C-C, Anseth KS. PEG hydrogels for the controlled release of biomolecules in regenerative medicine. Pharmaceut Res. 2009;26(3):631–43.
37. Hoffman MD, Van Hove AH, Benoit DS. Degradable hydrogels for spatiotemporal control of mesenchymal stem cells localized at decellularized bone allografts. Acta Biomater. 2014;10(8):3431–41. [PubMed: 24751534]
38. Park KM, Gerecht S. Harnessing developmental processes for vascular engineering and regeneration. Development. 2014;141(14):2760–9. [PubMed: 25005471]
39. Carmeliet P Mechanisms of angiogenesis and arteriogenesis. Nat Med. 2000;6(4):389. [PubMed: 10742145]
40. Koblizek TI, Weiss C, Yancopoulos GD, Deutsch U, Risau W. Angiopoietin-1 induces sprouting angiogenesis in vitro. Curr Biol. 1998;8(9):529–32. [PubMed: 9560344]
41. Shin Y, Jeon JS, Han S, Jung G-S, Shin S, Lee S-H, Sudo R, Kamm RD, Chung S. In vitro 3D collective sprouting angiogenesis under orchestrated ANG-1 and VEGF gradients. Lab Chip. 2011;11(13):2175–81. [PubMed: 21617793]
42. Wang L, Fan H, Zhang Z-Y, Lou A-J, Pei G-X, Jiang S, Mu T-W, Qin J-J, Chen S-Y, Jin D. Osteogenesis and angiogenesis of tissue-engineered bone constructed by prevascularized β-tricalcium phosphate scaffold and mesenchymal stem cells. Biomaterials. 2010;31(36):9452–61. [PubMed: 20869769]
43. Schindeler A, McDonald MM, Bokko P, Little DG, editors. Bone remodeling during fracture repair: The cellular picture. Semin Cell Dev Biol; 2008: Elsevier.
44. Kanczler J, Oreffo R. Osteogenesis and angiogenesis: the potential for engineering bone. Eur Cell Mater. 2008;15(2):100–14. [PubMed: 18454418]
45. Patrick AG, Ulijn RV. Hydrogels for the detection and management of protease levels. Macromol Biosci. 2010;10(10):1184–93. [PubMed: 20593363]
46. Patterson J, Hubbell JA. Enhanced proteolytic degradation of molecularly engineered PEG hydrogels in response to MMP-1 and MMP-2. Biomaterials. 2010;31(30):7836–45. [PubMed: 20667588]
47. Bracher M, Bezuidenhout D, Lutolf MP, Franz T, Sun M, Zilla P, Davies NH. Cell specific ingrowth hydrogels. Biomaterials. 2013;34(28):6797–803. [PubMed: 23777918]

Author Manuscript Author Manuscript Author Manuscript Author Manuscript

48. Taraboletti G, D'Ascenzo S, Borsotti P, Giavazzi R, Pavan A, Dolo V. Shedding of the matrix metalloproteinases MMP-2, MMP-9, and MT1-MMP as membrane vesicle-associated components by endothelial cells. Am J Pathol. 2002;160(2):673–80. [PubMed: 11839588]
49. Galliera E, Randelli P, Dogliotti G, Dozio E, Colombini A, Lombardi G, Cabitza P, Corsi M. Matrix metalloproteases MMP-2 and MMP-9: are they early biomarkers of bone remodelling and healing after arthroscopic acromioplasty? Injury. 2010;41(11):1204–7. [PubMed: 20950805]
50. Kumar S, Wan C, Ramaswamy G, Clemens TL, Ponnazhagan S. Mesenchymal stem cells expressing osteogenic and angiogenic factors synergistically enhance bone formation in a mouse model of segmental bone defect. Mol Ther. 2010;18(5):1026–34. [PubMed: 20068549]
51. Davis GE, Stratman AN, Sacharidou A, Koh W. Molecular basis for endothelial lumen formation and tubulogenesis during vasculogenesis and angiogenic sprouting. International review of cell and molecular biology: Elsevier; 2011. p. 101–65.
52. Chan ZC-K, Oentaryo MJ, Lee CW. MMP-mediated modulation of ECM environment during axonal growth and NMJ development. Neurosci Lett. 2020;724:134822. [PubMed: 32061716]
53. Wang L, Zhang ZG, Zhang RL, Gregg SR, Hozeska-Solgot A, LeTourneau Y, Wang Y, Chopp M. Matrix metalloproteinase 2 (MMP2) and MMP9 secreted by erythropoietin-activated endothelial cells promote neural progenitor cell migration. J Neurosci. 2006;26(22):5996–6003. [PubMed: 16738242]
54. Marrella A, Lee TY, Lee DH, Karuthedom S, Syla D, Chawla A, Khademhosseini A, Jang HL. Engineering vascularized and innervated bone biomaterials for improved skeletal tissue regeneration. Materials Today. 2018;21(4):362–76. [PubMed: 30100812]
55. Shubin AD, Felong TJ, Graunke D, Ovitt CE, Benoit DS. Development of poly (ethylene glycol) hydrogels for salivary gland tissue engineering applications. Tissue Engineering Part A. 2015;21(11–12):1733–51. [PubMed: 25762214]
56. Shubin AD, Felong TJ, Schutrum BE, Joe DS, Ovitt CE, Benoit DS. Encapsulation of primary salivary gland cells in enzymatically degradable poly (ethylene glycol) hydrogels promotes acinar cell characteristics. Acta Biomater. 2017;50:437–49. [PubMed: 28039063]
57. Van Hove AH, Beltejar M-JG, Benoit DS. Development and in vitro assessment of enzymatically-responsive poly (ethylene glycol) hydrogels for the delivery of therapeutic peptides. Biomaterials. 2014;35(36):9719–30. [PubMed: 25178558]
58. Fairbanks BD, Schwartz MP, Bowman CN, Anseth KS. Photoinitiated polymerization of PEG-diacrylate with lithium phenyl-2, 4, 6-trimethylbenzoylphosphinate: polymerization rate and cytocompatibility. Biomaterials. 2009;30(35):6702–7. [PubMed: 19783300]
59. Van Hove AH, Wilson BD, Benoit DS. Microwave-assisted functionalization of poly (ethylene glycol) and on-resin peptides for use in chain polymerizations and hydrogel formation. JoVE (Journal of Visualized Experiments). 2013(80):e50890. [PubMed: 24193366]
60. He YJ, Santana MF, Moucka M, Quirk J, Shuaibi A, Pimentel MB, Grossman S, Rashid MM, Cinar A, Georgiadis JG. Immobilized RGD concentration and Proteolytic Degradation Synergistically Enhance Vascular Sprouting within Hydrogel Scaffolds of Varying Modulus. J Biomater Sci Polym Ed. 2019(just-accepted):1–28.
61. He YJ, Santana MF, Moucka M, Quirk J, Shuaibi A, Pimentel MB, Grossman S, Rashid MM, Cinar A, Georgiadis JG. Immobilized RGD concentration and proteolytic degradation synergistically enhance vascular sprouting within hydrogel scaffolds of varying modulus. Journal of Biomaterials Science, Polymer Edition. 2020;31(3):324–49. [PubMed: 31774730]
62. Peters EB, Christoforou N, Leong KW, Truskey GA, West JL. Poly (ethylene glycol) hydrogel scaffolds containing cell-adhesive and protease-sensitive peptides support microvessel formation by endothelial progenitor cells. Cellular and molecular bioengineering. 2016;9(1):38–54. [PubMed: 27042236]
63. Au P, Tam J, Fukumura D, Jain RK. Bone marrow–derived mesenchymal stem cells facilitate engineering of long-lasting functional vasculature. Blood, The Journal of the American Society of Hematology. 2008;111(9):4551–8.
64. Malcolm DW, Varghese JJ, Sorrells JE, Ovitt CE, Benoit DS. The effects of biological fluids on colloidal stability and siRNA delivery of a pH-responsive micellar nanoparticle delivery system. ACS nano. 2018;12(1):187–97. [PubMed: 29232104]

Author Manuscript Author Manuscript Author Manuscript Author Manuscript

65. Charvat S, Le Griel C, Chignol M-C, Schmitt D, Serres M. Ras-transfection up-regulated HaCaT cell migration: inhibition by Marimastat. Clin Exp Metastas. 1999;17(8):677–85.
66. Tonn JC, Kerkau S, Hanke A, Bouterfa H, Mueller JG, Wagner S, Vince GH, Roosen K. Effect of synthetic matrix-metalloproteinase inhibitors on invasive capacity and proliferation of human malignant gliomas in vitro. Int J Cancer. 1999;80(5):764–72. [PubMed: 10048980]
67. Zhu W-H, Guo X, Villaschi S, Nicosia RF. Regulation of vascular growth and regression by matrix metalloproteinases in the rat aorta model of angiogenesis. Lab Invest. 2000;80(4):545–55. [PubMed: 10780671]
68. Feigenson M, Eliseev RA, Jonason JH, Mills BN, O'Keefe RJ. PGE2 receptor subtype 1 (EP1) regulates mesenchymal stromal cell osteogenic differentiation by modulating cellular energy metabolism. J Cell Biochem. 2017;118(12):4383–93. [PubMed: 28444901]
69. Wang Y, Newman MR, Ackun-Farmmer M, Baranello MP, Sheu T-J, Puzas JE, Benoit DS. Fracture-targeted delivery of β-catenin agonists via peptide-functionalized nanoparticles augments fracture healing. ACS Nano. 2017;11(9):9445–58. [PubMed: 28881139]
70. Stolzing A, Jones E, McGonagle D, Scutt A. Age-related changes in human bone marrow-derived mesenchymal stem cells: consequences for cell therapies. Mech Ageing Dev. 2008;129(3):163–73. [PubMed: 18241911]
71. Matsuzaki Y, Umemoto T, Tanaka Y, Okano T, Yamato M. β2-Microglobulin is an appropriate reference gene for RT-PCR-based gene expression analysis of hematopoietic stem cells. Regenerative Therapy. 2015;1:91–7. [PubMed: 31245448]
72. Valenti MT, Dalle Carbonare L, Donatelli L, Bertoldo F, Zanatta M, Cascio VL. Gene expression analysis in osteoblastic differentiation from peripheral blood mesenchymal stem cells. Bone. 2008;43(6):1084–92. [PubMed: 18761114]
73. Dalby MJ, Gadegaard N, Tare R, Andar A, Riehle MO, Herzyk P, Wilkinson CD, Oreffo RO. The control of human mesenchymal cell differentiation using nanoscale symmetry and disorder. Nat Mater. 2007;6(12):997. [PubMed: 17891143]
74. Kumar S, Mahendra G, Ponnazhagan S. Determination of osteoprogenitor-specific promoter activity in mouse mesenchymal stem cells by recombinant adeno-associated virus transduction. Biochimica et Biophysica Acta (BBA)-Gene Structure and Expression. 2005;1731(2):95–103. [PubMed: 16225939]
75. Kong X, Liu Y, Ye R, Zhu B, Zhu Y, Liu X, Hu C, Luo H, Zhang Y, Ding Y. GSK3β is a checkpoint for TNF-α-mediated impaired osteogenic differentiation of mesenchymal stem cells in inflammatory microenvironments. Biochimica et Biophysica Acta (BBA)-General Subjects. 2013;1830(11):5119–29. [PubMed: 23911749]
76. Tiyapatanaputi P, Rubery PT, Carmouche J, Schwarz EM, O'Keefe RJ, Zhang X. A novel murine segmental femoral graft model. J Orthopaed Res. 2004;22(6):1254–60.
77. Burwell RG. STUDIES IN THE TRANSPLANTATION OF BONE VII. The Fresh Composite Homograft-Autograft of Cancellous Bone. The Journal of bone and joint surgery British volume. 1964;46(1):110–40. [PubMed: 14126228]
78. Reynolds DG, Takahata M, Lerner AL, O'Keefe RJ, Schwarz EM, Awad HA. Teriparatide therapy enhances devitalized femoral allograft osseointegration and biomechanics in a murine model. Bone. 2011;48(3):562–70. [PubMed: 20950720]
79. Raina DB, Qayoom I, Larsson D, Zheng MH, Kumar A, Isaksson H, Lidgren L, Tägil M. Guided tissue engineering for healing of cancellous and cortical bone using a combination of biomaterial based scaffolding and local bone active molecule delivery. Biomaterials. 2019;188:38–49. [PubMed: 30321863]
80. Hoffman MD, Xie C, Zhang X, Benoit DS. The effect of mesenchymal stem cells delivered via hydrogel-based tissue engineered periosteum on bone allograft healing. Biomaterials. 2013;34(35):8887–98. doi: 10.1016/j.biomaterials.2013.08.005. [PubMed: 23958029]
81. Hoffman MD, Benoit DS. Emulating native periosteum cell population and subsequent paracrine factor production to promote tissue engineered periosteum-mediated allograft healing. Biomaterials. 2015;52:426–40. [PubMed: 25818449]

Author Manuscript Author Manuscript Author Manuscript Author Manuscript

82. Zhang L, Chang M, Beck CA, Schwarz EM, Boyce BF. Analysis of new bone, cartilage, and fibrosis tissue in healing murine allografts using whole slide imaging and a new automated histomorphometric algorithm. Bone research. 2016;4(1):1–9.
83. Filipowska J, Tomaszewski KA, Niedźwiedzki Ł, Walocha JA, Niedźwiedzki T. The role of vasculature in bone development, regeneration and proper systemic functioning. Angiogenesis. 2017;20(3):291–302. [PubMed: 28194536]
84. Ramasamy SK, Kusumbe AP, Wang L, Adams RH. Endothelial Notch activity promotes angiogenesis and osteogenesis in bone. Nature. 2014;507(7492):376–80. [PubMed: 24647000]
85. Shen Q, Goderie SK, Jin L, Karanth N, Sun Y, Abramova N, Vincent P, Pumiglia K, Temple S. Endothelial cells stimulate self-renewal and expand neurogenesis of neural stem cells. Science. 2004;304(5675):1338–40. [PubMed: 15060285]
86. Doke SK, Dhawale SC. Alternatives to animal testing: A review. Saudi Pharmaceutical Journal. 2015;23(3):223–9. [PubMed: 26106269]
87. Salman RA-S, Beller E, Kagan J, Hemminki E, Phillips RS, Savulescu J, Macleod M, Wisely J, Chalmers I. Increasing value and reducing waste in biomedical research regulation and management. The Lancet. 2014;383(9912):176–85.
88. Charan J, Kantharia N. How to calculate sample size in animal studies? Journal of pharmacology & pharmacotherapeutics. 2013;4(4):303. [PubMed: 24250214]
89. Yang G, Mahadik B, Choi JY, Fisher JP. Vascularization in tissue engineering: fundamentals and state-of-art. Progress in Biomedical Engineering. 2020;2(1):012002.
90. Tetzlaff F, Fischer A. Human endothelial cell Spheroid-based sprouting angiogenesis assay in collagen. Bio-Protocol. 2018;8:e2995.
91. Lu C, Marcucio R, Miclau T. Assessing angiogenesis during fracture healing. The Iowa orthopaedic journal. 2006;26:17. [PubMed: 16789443]
92. Weiss S, Zimmermann G, Pufe T, Varoga D, Henle P. The systemic angiogenic response during bone healing. Arch Orthop Traum Su. 2009;129(7):989–97.
93. Aoki M, Tamai K, Saotome K. Substance P-and calcitonin gene-related peptide-immunofluorescent nerves in the repair of experimental bone defects. Int Orthop. 1994;18(5):317–24. [PubMed: 7531673]
94. Liu S, Jin D, Wu J-q, Xu Z-y, Fu S, Mei G, Zou Z-L, Ma S-h. Neuropeptide Y stimulates osteoblastic differentiation and VEGF expression of bone marrow mesenchymal stem cells related to canonical Wnt signaling activating in vitro. Neuropeptides. 2016;56:105–13. [PubMed: 26707636]
95. Koefoed M, Ito H, Gromov K, Reynolds DG, Awad HA, Rubery PT, Ulrich-Vinther M, Soballe K, Guldberg RE, Lin AS. Biological effects of rAAV-caAlk2 coating on structural allograft healing. Mol Ther. 2005;12(2):212–8. [PubMed: 16043092]
96. Betz OB, Betz VM, Schröder C, Penzkofer R, Göttlinger M, Mayer-Wagner S, Augat P, Jansson V, Müller PE. Repair of large segmental bone defects: BMP-2 gene activated muscle grafts vs. autologous bone grafting. BMC biotechnology. 2013;13(1):65. [PubMed: 23927083]
97. Morgan EF, De Giacomo A, Gerstenfeld LC. Overview of skeletal repair (fracture healing and its assessment). Skeletal Development and Repair: Springer; 2014. p. 13–31.
98. Casanova M, Schindeler A, Little D, Müller R, Schneider P. Quantitative phenotyping of bone fracture repair: a review. BoneKEy reports. 2014;3.
99. Roberts TT, Rosenbaum AJ. Bone grafts, bone substitutes and orthobiologics: the bridge between basic science and clinical advancements in fracture healing. Organogenesis. 2012;8(4):114–24. [PubMed: 23247591]
100. Wong SA, Rivera KO, Miclau T III, Alsberg E, Marcucio RS, Bahney CS. Microenvironmental regulation of chondrocyte plasticity in endochondral repair—a new frontier for developmental engineering. Frontiers in bioengineering and biotechnology. 2018;6:58. [PubMed: 29868574]
101. Gerstenfeld LC, Cullinane DM, Barnes GL, Graves DT, Einhorn TA. Fracture healing as a post-natal developmental process: molecular, spatial, and temporal aspects of its regulation. J Cell Biochem. 2003;88(5):873–84. [PubMed: 12616527]
102. Marsell R, Einhorn TA. The biology of fracture healing. Injury. 2011;42(6):551–5. [PubMed: 21489527]

Author Manuscript Author Manuscript Author Manuscript Author Manuscript

103. Hu K, Olsen BR. The roles of vascular endothelial growth factor in bone repair and regeneration. Bone. 2016;91:30–8. [PubMed: 27353702]
104. Hankenson KD, Dishowitz M, Gray C, Schenker M. Angiogenesis in bone regeneration. Injury. 2011;42(6):556–61. [PubMed: 21489534]
105. Maes C, Kobayashi T, Selig MK, Torrekens S, Roth SI, Mackem S, Carmeliet G, Kronenberg HM. Osteoblast precursors, but not mature osteoblasts, move into developing and fractured bones along with invading blood vessels. Dev Cell. 2010;19(2):329–44. [PubMed: 20708594]
106. Jiang X, Xu C, Shi H, Cheng Q. PTH1–34 improves bone healing by promoting angiogenesis and facilitating MSCs migration and differentiation in a stabilized fracture mouse model. PLoS ONE. 2019;14(12).
107. Carmeliet P Blood vessels and nerves: common signals, pathways and diseases. Nat Rev Genet. 2003;4(9):710. [PubMed: 12951572]
108. Carmeliet P, Tessier-Lavigne M. Common mechanisms of nerve and blood vessel wiring. Nature. 2005;436(7048):193–200. [PubMed: 16015319]
109. Stegen S, van Gastel N, Carmeliet G. Bringing new life to damaged bone: the importance of angiogenesis in bone repair and regeneration. Bone. 2015;70:19–27. [PubMed: 25263520]
110. El Backly RM, Zaky SH, Muraglia A, Tonachini L, Brun F, Canciani B, Chiapale D, Santolini F, Cancedda R, Mastrogiacomo M. A platelet-rich plasma-based membrane as a periosteal substitute with enhanced osteogenic and angiogenic properties: a new concept for bone repair. Tissue Engineering Part A. 2013;19(1–2):152–65. [PubMed: 22849574]
111. Zhao L, Zhao J, Wang S, Wang J, Liu J. Comparative study between tissue-engineered periosteum and structural allograft in rabbit critical-sized radial defect model. J Biomed Mater Res Part B Appl Biomater. 2011;97(1):1–9.
112. Shi X, Chen S, Zhao Y, Lai C, Wu H. Enhanced osteogenesis by a biomimic pseudo-periosteum-involved tissue engineering Strategy. Advanced healthcare materials. 2013;2(9):1229–35. [PubMed: 23495244]
113. Jacinto A, Wolpert L. Filopodia. Curr Biol. 2001;11(16):R634. [PubMed: 11525752]
114. Wang Y, Malcolm DW, Benoit DS. Controlled and sustained delivery of siRNA/NPs from hydrogels expedites bone fracture healing. Biomaterials. 2017;139:127–38. [PubMed: 28601703]
115. GE D Senger DR. Endothelial extracellular matrix: biosynthesis, remodeling, and functions during vascular morphogenesis and neovessel stabilization. Circ Res. 2005;97:1093–107. [PubMed: 16306453]
116. Saunders WB, Bayless KJ, Davis GE. MMP-1 activation by serine proteases and MMP-10 induces human capillary tubular network collapse and regression in 3D collagen matrices. J Cell Sci. 2005;118(10):2325–40. [PubMed: 15870107]
117. Bergers G, Brekken R, McMahon G, Vu TH, Itoh T, Tamaki K, Tanzawa K, Thorpe P, Itohara S, Werb Z. Matrix metalloproteinase-9 triggers the angiogenic switch during carcinogenesis. Nat Cell Biol. 2000;2(10):737–44. [PubMed: 11025665]
118. Holmbeck K, Bianco P, Caterina J, Yamada S, Kromer M, Kuznetsov SA, Mankani M, Robey PG, Poole AR, Pidoux I. MT1-MMP-deficient mice develop dwarfism, osteopenia, arthritis, and connective tissue disease due to inadequate collagen turnover. Cell. 1999;99(1):81–92. [PubMed: 10520996]
119. Zhou Z, Apte SS, Soininen R, Cao R, Baaklini GY, Rauser RW, Wang J, Cao Y, Tryggvason K. Impaired endochondral ossification and angiogenesis in mice deficient in membrane-type matrix metalloproteinase I. Proc Natl Acad Sci. 2000;97(8):4052–7. [PubMed: 10737763]
120. Vu TH, Shipley JM, Bergers G, Berger JE, Helms JA, Hanahan D, Shapiro SD, Senior RM, Werb Z. MMP-9/gelatinase B is a key regulator of growth plate angiogenesis and apoptosis of hypertrophic chondrocytes. Cell. 1998;93(3):411–22. [PubMed: 9590175]
121. Verslegers M, Lemmens K, Van Hove I, Moons L. Matrix metalloproteinase-2 and-9 as promising benefactors in development, plasticity and repair of the nervous system. Prog Neurobiol. 2013;105:60–78. [PubMed: 23567503]
122. Hehr CL, Hocking JC, McFarlane S. Matrix metalloproteinases are required for retinal ganglion cell axon guidance at select decision points. Development. 2005;132(15):3371–9. [PubMed: 15975939]

Author Manuscript Author Manuscript Author Manuscript Author Manuscript

123. Linden GJ, Irwin CR, Lundy FT. Neuropeptides regulate expression of angiogenic growth factors in human dental pulp fibroblasts. J Endod. 2009;35(6):829–33. [PubMed: 19482180]

124. Fang Z, Yang Q, Xiong W, Li G-h, Liao H, Xiao J, Li F. Effect of CGRP-adenoviral vector transduction on the osteoblastic differentiation of rat adipose-derived stem cells. PloS one. 2013;8(8).

125. Mukohyama H, Ransjö M, Taniguchi H, Ohyama T, Lerner UH. The inhibitory effects of vasoactive intestinal peptide and pituitary adenylate cyclase-activating polypeptide on osteoclast formation are associated with upregulation of osteoprotegerin and downregulation of RANKL and RANK. Biochem Bioph Res Co. 2000;271(1):158–63.

126. Cornish J, Callon K, Lin CQ, Xiao C, Gamble G, Cooper G, Reid I. Comparison of the effects of calcitonin gene-related peptide and amylin on osteoblasts. J Bone Miner Res. 1999;14(8):1302–9. [PubMed: 10457262]

127. Honma Y, Araki T, Gianino S, Bruce A, Heuckeroth R, Johnson E, Milbrandt J. Artemin is a vascular-derived neurotropic factor for developing sympathetic neurons. Neuron. 2002;35(2):267–82. Epub 2002/08/06. doi: 10.1016/s0896-6273(02)00774-2. [PubMed: 12160745]

128. Kuruvilla R, Zweifel LS, Glebova NO, Lonze BE, Valdez G, Ye H, Ginty DD. A neurotrophin signaling cascade coordinates sympathetic neuron development through differential control of TrkA trafficking and retrograde signaling. Cell. 2004;118(2):243–55. Epub 2004/07/21. doi: 10.1016/j.cell.2004.06.021. [PubMed: 15260993]

129. Carmeliet P Blood vessels and nerves: common signals, pathways and diseases. Nat Rev Genet. 2003;4(9):710–20. [PubMed: 12951572]

130. Carano RA, Filvaroff EH. Angiogenesis and bone repair. Drug Discov Today. 2003;8(21):980–9. [PubMed: 14643161]

131. Prokoph S, Chavakis E, Levental KR, Zieris A, Freudenberg U, Dimmeler S, Werner C. Sustained delivery of SDF-1α from heparin-based hydrogels to attract circulating pro-angiogenic cells. Biomaterials. 2012;33(19):4792–800. [PubMed: 22483246]

132. Benoit DS, Schwartz MP, Durney AR, Anseth KS. Small functional groups for controlled differentiation of hydrogel-encapsulated human mesenchymal stem cells. Nature materials. 2008;7(10):816–23. doi: 10.1038/nmat2269. [PubMed: 18724374]

133. Nuttelman CR, Tripodi MC, Anseth KS. In vitro osteogenic differentiation of human mesenchymal stem cells photoencapsulated in PEG hydrogels. J Biomed Mater Res A. 2004;68(4):773–82. doi: 10.1002/jbm.a.20112. [PubMed: 14986332]

134. Weber LM, Anseth KS. Hydrogel encapsulation environments functionalized with extracellular matrix interactions increase islet insulin secretion. Matrix biology : journal of the International Society for Matrix Biology. 2008;27(8):667–73. doi: 10.1016/j.matbio.2008.08.001. [PubMed: 18773957]

135. Rundhaug JE. Matrix metalloproteinases, angiogenesis, and cancer: commentary re: Lockhart AC et al., Reduction of wound angiogenesis in patients treated with BMS-275291, a broad spectrum matrix metalloproteinase inhibitor. Clin. Cancer Res, 9: 00–00, 2003. Clin Cancer Res. 2003;9(2):551–4. [PubMed: 12576417]

136. Rundhaug JE. Matrix metalloproteinases and angiogenesis. J Cell Mol Med. 2005;9(2):267–85. [PubMed: 15963249]

137. Langen UH, Pitulescu ME, Kim JM, Enriquez-Gasca R, Sivaraj KK, Kusumbe AP, Singh A, Di Russo J, Bixel MG, Zhou B, Sorokin L, Vaquerizas JM, Adams RH. Cell-matrix signals specify bone endothelial cells during developmental osteogenesis. Nat Cell Biol. 2017;19(3):189–201. Epub 2017/02/22. doi: 10.1038/ncb3476. [PubMed: 28218908]

138. Nagase H, Fields GB. Human matrix metalloproteinase specificity studies using collagen sequence-based synthetic peptides. Biopolymers. 1996;40(4):399–416. doi: Doi 10.1002/(Sici)1097-0282(1996)40:4<399::Aid-Bip5>3.0.Co;2-R. [PubMed: 8765610]

139. Turk BE, Huang LL, Piro ET, Cantley LC. Determination of protease cleavage site motifs using mixture-based oriented peptide libraries. Nat Biotechnol. 2001;19(7):661–7. [PubMed: 11433279]

Author Manuscript Author Manuscript Author Manuscript Author Manuscript

140. Sawhney AS, Pathak CP, Hubbell JA. Bioerodible Hydrogels Based on Photopolymerized Poly(Ethylene Glycol)-Co-Poly(Alpha-Hydroxy Acid) Diacrylate Macromers. Macromolecules. 1993;26(4):581–7.

141. Alvarez R, Lee H-L, Wang C-Y, Hong C. Characterization of the osteogenic potential of mesenchymal stem cells from human periodontal ligament based on cell surface markers. International journal of oral science. 2015;7(4):213–9. [PubMed: 26674423]

142. Nusspaumer G, Jaiswal S, Barbero A, Reinhardt R, Ronen DI, Haumer A, Lufkin T, Martin I, Zeller R. Ontogenic identification and analysis of mesenchymal stromal cell populations during mouse limb and long bone development. Stem cell reports. 2017;9(4):1124–38. [PubMed: 28919259]

Author Manuscript Author Manuscript Author Manuscript Author Manuscript

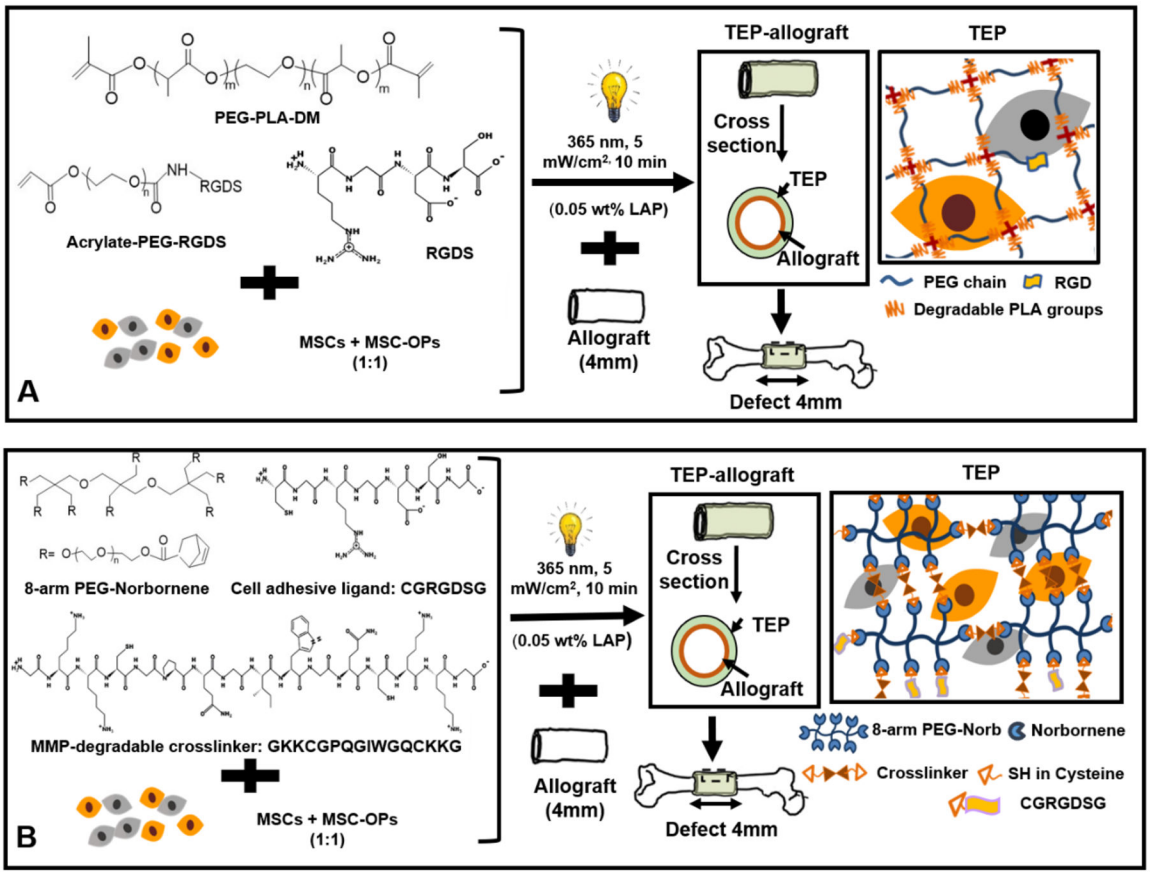

Figure 1.

Scheme of (A) Hydro-TEP: MSCs and OPs (at 1:1 ratio) were encapsulated in hydrolytically degradable PEG-PLA-DM hydrogel where Acrylate-PEG-RGDS was used as cell adhesion ligand, and (B) MMP-TEP: MSCs and OPs (at 1:1 ratio) were encapsulated in PEG-norbornene hydrogel where MDC and CGRGDSG were used as MMP-degradable crosslinker and cell adhesion ligand, respectively.

Author Manuscript Author Manuscript Author Manuscript Author Manuscript

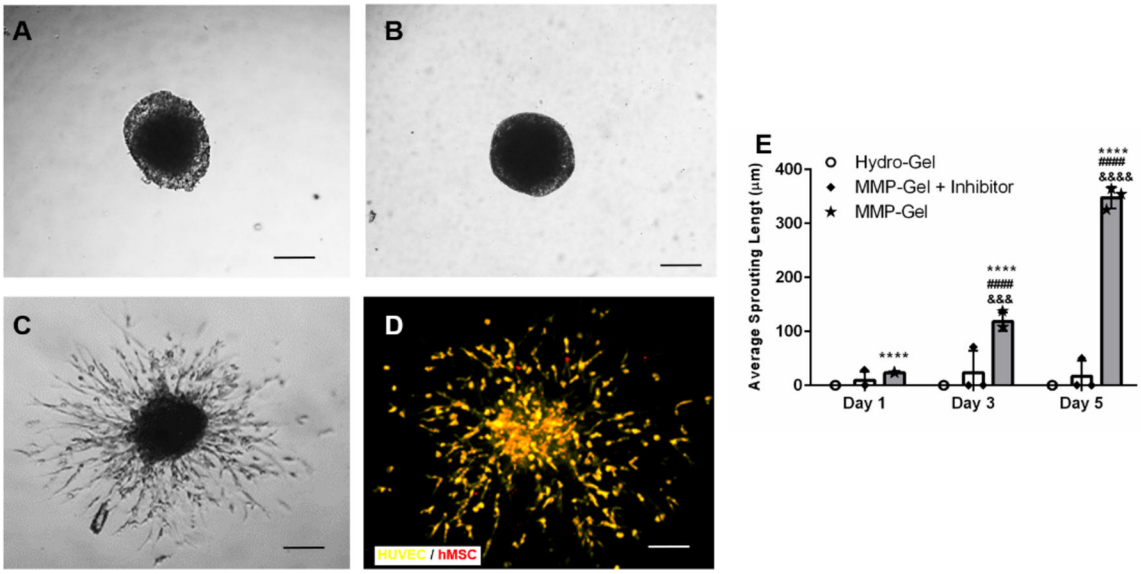

Figure 2.

Representative images of HUVEC/hMSC spheroids within (A) hydrolytically degradable hydrogels (Hydro-Gel), (B, C and D) MMP-degradable hydrogels (MMP-Gel) with and without MMP inhibitor respectively after 5 days. Confocal microscopy (D) illustrates that HUVECs and hMSCs concomitantly sprouted in MMP-Gel. (E) Cell sprouting in different gels was quantified as average sprouting length after 1, 3, and 5 days using one-way ANOVA with Dunnett's post-hoc analysis, where $n = 3$, scale bar = 200 µm, $p < 0.0001$ indicates significant differences compared to Hydro-Gel (****) and MMP-Gel plus inhibitor (####) at the same time points and, $p < 0.001$ and $p < 0.0001$ indicates significant differences between same type of gel at different time points (&&&, &&&&).

Author Manuscript Author Manuscript Author Manuscript Author Manuscript

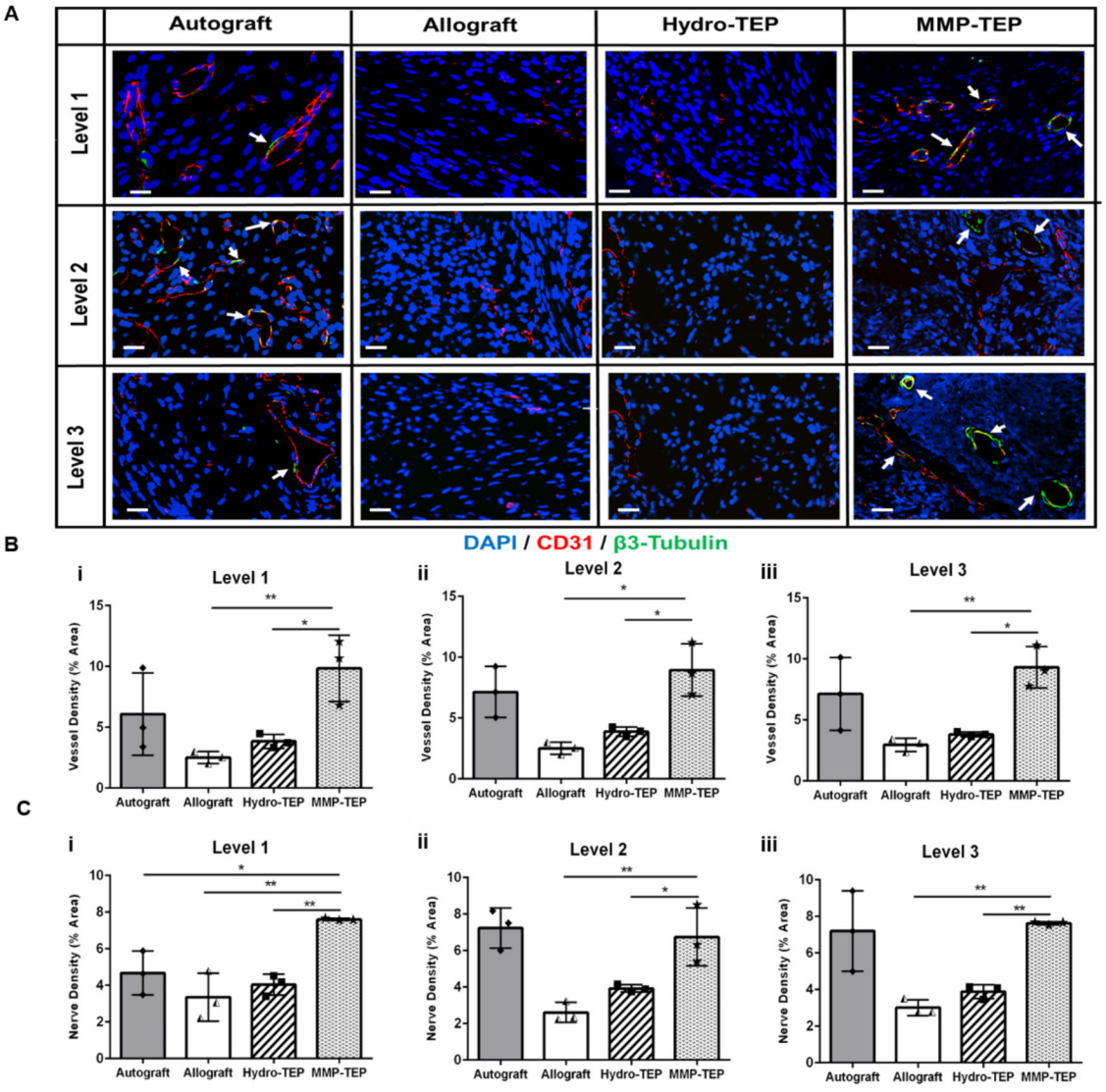

Figure 3.

(A) Representative confocal images of co-stained of CD31 (blood vessels, red) and β3-tubulin (nerves, green) on the crossections of allograft at levels proximal (Supplemental Fig. 1, Level 1), medial (Supplemental Fig. 1, Level 2), and distal (Supplemental Fig. 1, Level 3) in relation to the femoral head (scale bar = 20 μm). (B-C) Quantification of blood vesssel and nerve density in three levels repectively using one-way ANOVA with Dunnett's post-hoc analysis, where $n = 3$, $p < 0.05$, $p < 0.01$, $p < 0.001$, $p < 0.001$ indicates significance compared to MMP-TEP (*, **, ***, ****).

Author Manuscript Author Manuscript Author Manuscript Author Manuscript

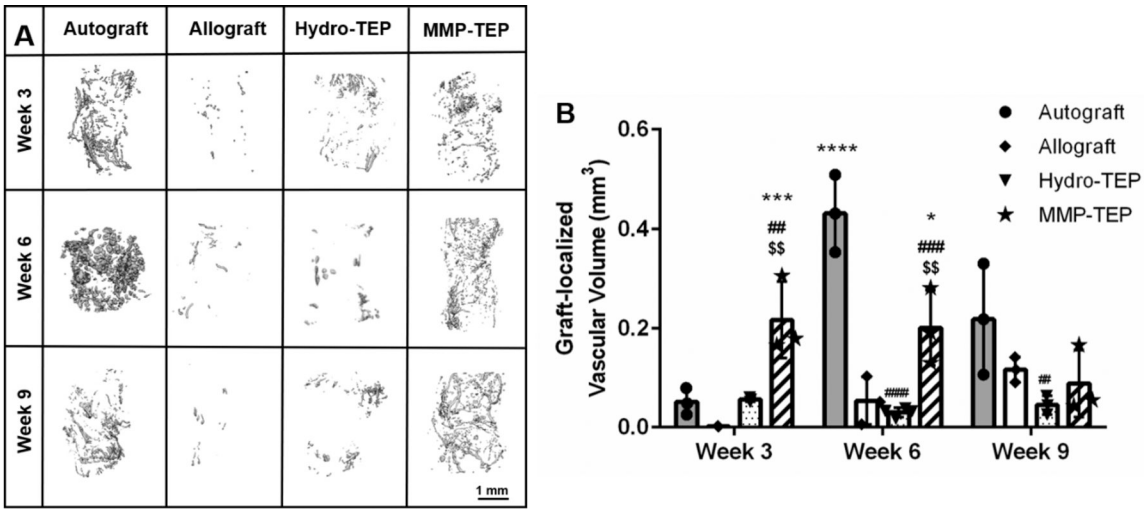

Figure 4.

(A) Representative μCT images and (B) quantification of graft-localized vascularization for autografts, allografts, and TEP-modified allografts at 3, 6, and 9 weeks post-surgery (B) using two-way ANOVA with Tukey's post-hoc analysis, where $n = 3–4$, error bars represent standard deviation; $p < 0.05$, $p < 0.01$, $p < 0.001$, $p < 0.00001$, indicates significance compared to allograft (*, **, ***, ****), autograft (#, ##, ###, ####) and Hydro-TEP ($, $$, $$$, $$$$).

Author Manuscript Author Manuscript Author Manuscript Author Manuscript

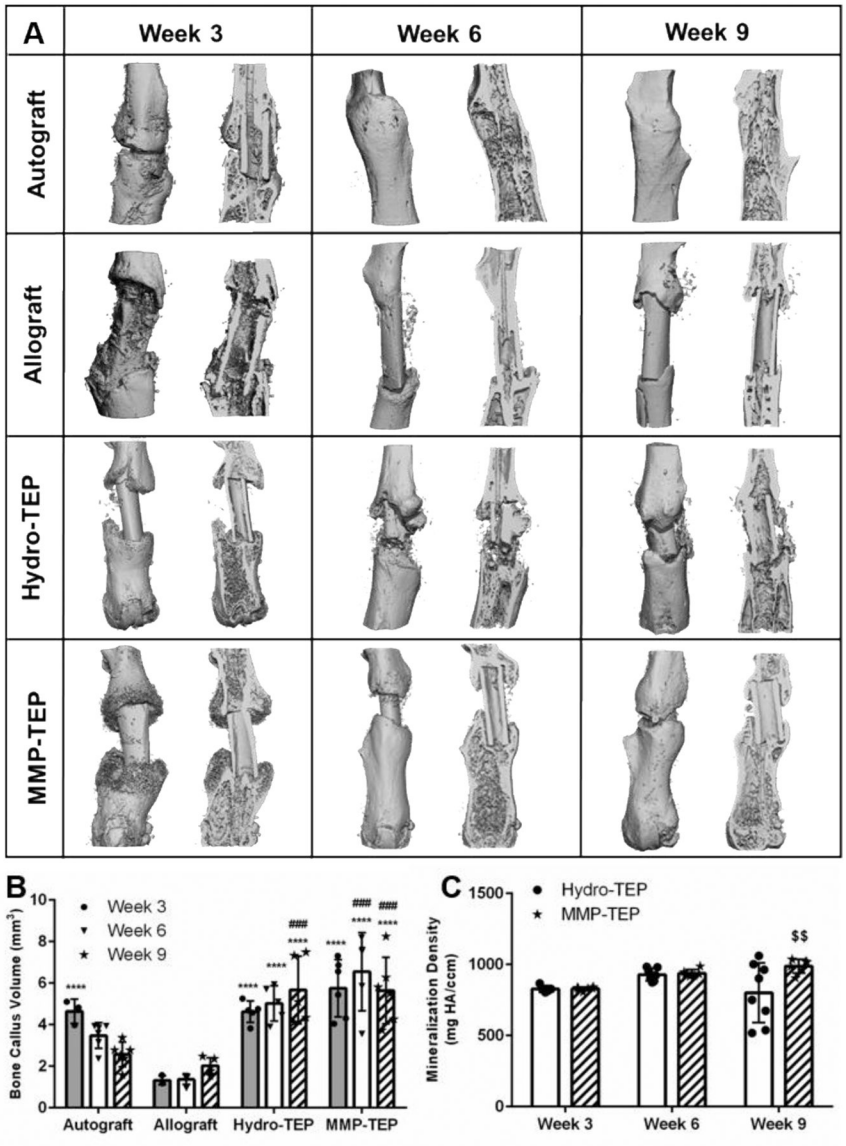

Figure 5.

Bone callus formation at 3, 6, and 9 weeks post-surgery were measured using μCT: (A) reconstructed images of bone callus in both intact and sagittal cut views; subsequent quantification of (B) volume and (C) mineralization density of bone callus using two-way ANOVA with Tukey's post-hoc analysis, where $n = 5–6$; error bars represent standard deviation; $p < 0.001$ and $p < 0.0001$ indicates significance compared to allograft (***, ****), autograft (###, ####) and Hydro-TEP ($p < 0.01$, $$)). (Images and data for autograft, allograft, and Hydro-TEP callus volume and mineralization after 6 and 9 weeks are derived from our previous study[29].)

Author Manuscript Author Manuscript Author Manuscript Author Manuscript

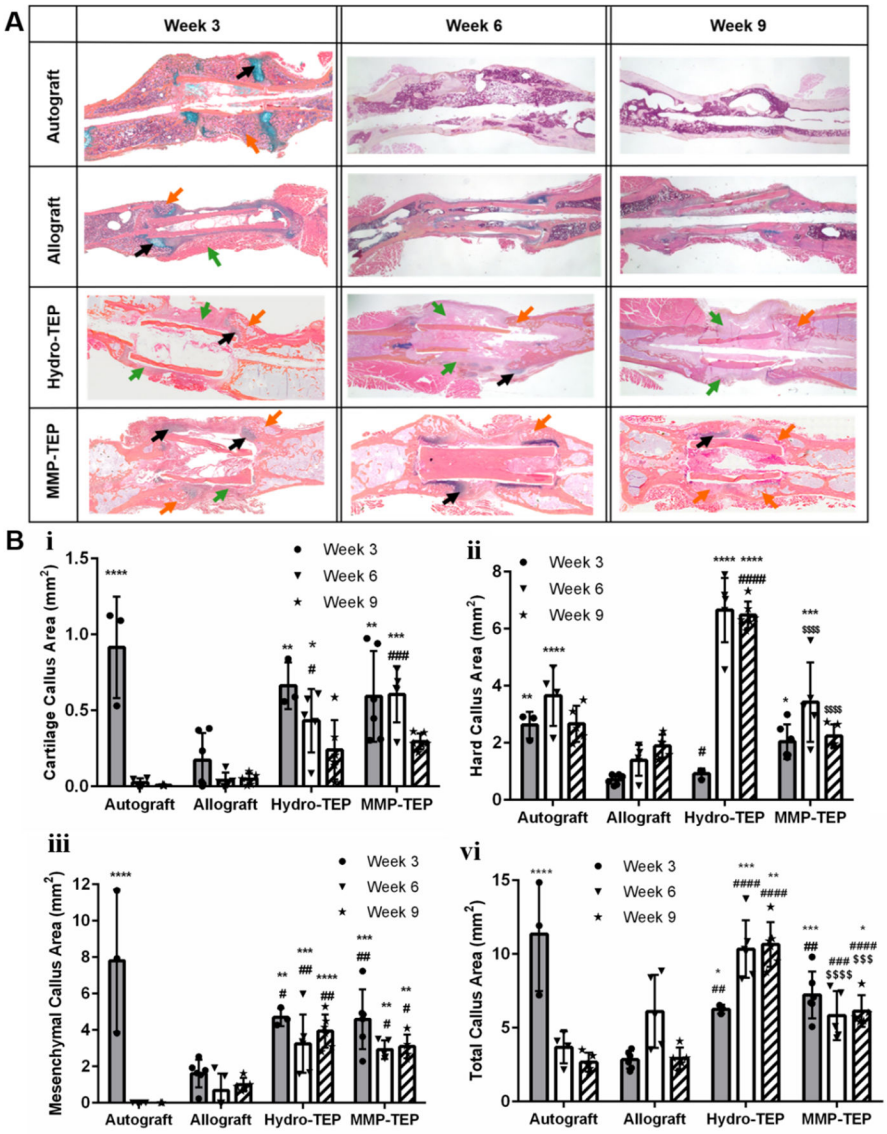

Figure 6.

Representative images (A) and quantification of callus area (B) using two-way ANOVA with Tukey's post-hoc analysis, where $n = 3–6$; error bars represent standard deviation; $p < 0.05$, $p < 0.01$, $p < 0.001$, and $p < 0.0001$ indicate significances compared to allograft (*, **, ***, ****), autograft (#, ##, ###, ####) and Hydro-TEP ($$$$$)). Histological analysis of grafted femur sections was performed using Alcian Blue (blue: glycosaminoglycans and proteoglycans, black arrow) and Orange G staining (orange: bone; pink: surrounding fibrotic tissue, orange arrow), where green arrow indicates mesenchymal callus (some quantification data are derived from our previously study[29].)

Author Manuscript

Author Manuscript

Author Manuscript

Author Manuscript

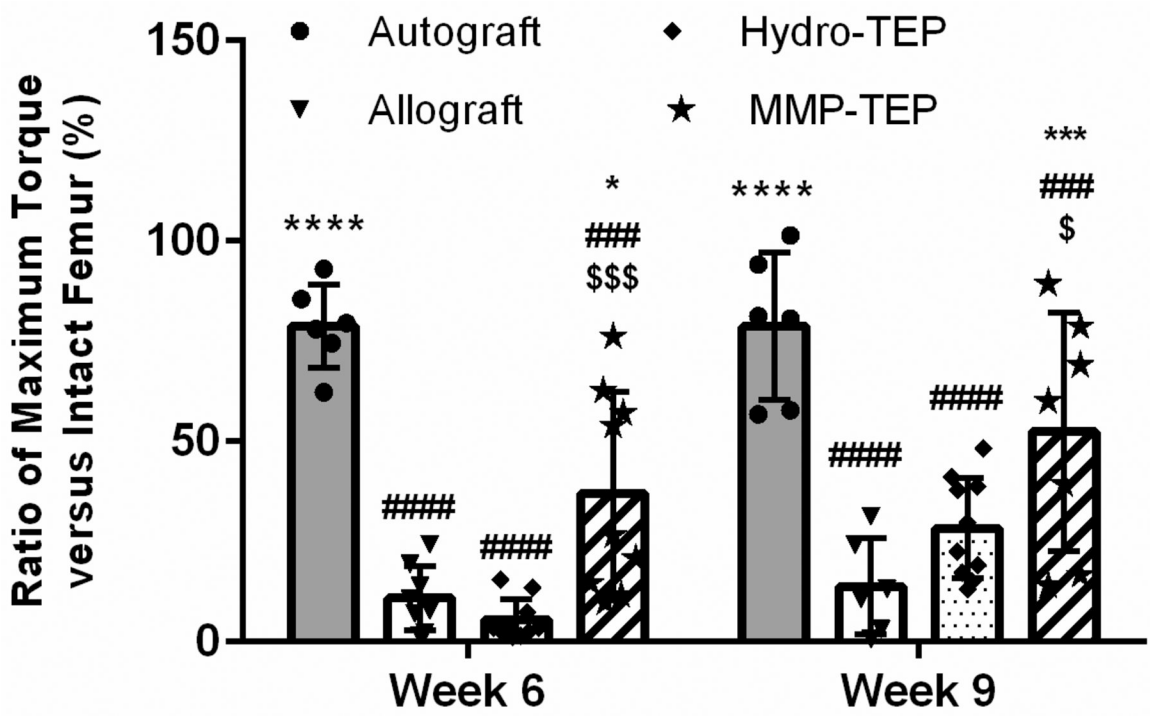

Figure 7.

Maximum torque of autogtaft, allograft, and TEP-modified allografts compared to intact femurs after 6 and 9 weeks using two-way ANOVA with Tukey's post-hoc analysis, where n = 6–8 and $p < 0.05$, $p < 0.001$, $p < 0.0001$ indicates significance compared to allograft (*, ***, ****), autograft (#, ###, ####) and Hydro-TEP ($, $$$, $$$$)). (Some comparison data are derived from our previous study[29]).